Pharmacological Research 135 (2018) 239–258

Contents lists available at ScienceDirect

Pharmacological Research

journal homepage: www.elsevier.com/locate/yphrs

Invited Review

Targeting oncogenic Raf protein-serine/threonine kinases in human cancers

Robert Roskoski Jr.

Blue Ridge Institute for Medical Research, 3754 Brevard Road, Suite 116, Box 19, Horse Shoe, North Carolina 28742-8814, United States

ARTICLE INFO

Chemical compounds studied in this article:
Binimetinib (PubMED CID: 10288191)
Cobimetanib (PubMED CID: 16222096)
Dabrafenib: (PubMED CID: 44462760)
Encorafenib: (PubMED CID 50922675)
Lifirafenib: (PubMED CID:89670174)
LY3009120 (PubMED CID: 71721540)
PLX7904: (PubMED CID: 901169945)
Sorafenib: (PubMED CID: 216239)
Trametinib (PubMED CID: 11707110)
Vemurafenib: (PubMED CID: 42611257)

Keywords:
Catalytic spine
K/E/D/D
Melanoma
Protein kinase inhibitor classification
Protein kinase structure
Targeted cancer therapy

ABSTRACT

The Ras-Raf-MEK-ERK signal transduction cascade is arguably the most important oncogenic pathway in human cancers. Ras-GTP promotes the formation of active homodimers or heterodimers of A-Raf, B-Raf, and C-Raf by an intricate process. These enzymes are protein-serine/threonine kinases that catalyze the phosphorylation and activation of MEK1 and MEK2 which, in turn, catalyze the phosphorylation and activation of ERK1 and ERK2. The latter catalyze the regulatory phosphorylation of dozens of cytosolic and nuclear proteins. The X-ray crystal structure of B-Raf–MEK1 depicts a face-to-face dimer with interacting activation segments; B-Raf is in an active conformation and MEK1 is in an inactive conformation. Besides the four traditional components in the Ras-Raf-MEK-ERK signaling module, scaffolding proteins such as Kinase Suppressor of Ras (KSR1/2) play an important role in this signaling cascade by functioning as a scaffold protein. *RAS* mutations occur in about 30% of all human cancers. Moreover, $BRAF^{V600E}$ mutations occur in about 8% of all cancers making this the most prevalent oncogenic protein kinase. Vemurafenib and dabrafenib are $B\text{-}Raf^{V600E}$ inhibitors that were approved for the treatment of melanomas bearing the V600E mutation. Coupling MEK1/2 inhibitors with B-Raf inhibitors is more effective in treating such melanomas and dual therapy is now the standard of care. Vemurafenib and cobimetanib, dabrafenib and trametinib, and encorafenib plus binimetinib are the FDA-approved combinations for the treatment of $BRAF^{V600E}$ melanomas. Although such mutations occur in other neoplasms including thyroid, colorectal, and non-small cell lung cancers, these agents are not as effective in treating these non-melanoma neoplasms. Vemurafenib and dabrafenib produce the paradoxical activation of the MAP kinase pathway in wild type *BRAF* cells. The precise mechanism for this activation is unclear, but drug-induced Raf activating side-to-side dimerization appears to be an essential step. Although 63%–76% of all people with advanced melanoma with the $BRAF^{V600E}$ mutation derive clinical benefit from combination therapy, median progression-free survival lasts only about nine months and 90% of patients develop resistance within one year. The various secondary resistance mechanisms include *NRAS* or *KRAS* mutations (20%), *BRAF* splice variants (16%), $BRAF^{V600E/K}$ amplifications (13%), *MEK1/2* mutations (7%), and non-MAP kinase pathway alterations (11%). Vemurafenib and dabrafenib bind to an inactive form of B-Raf (αC-helix$_{out}$ and DFG-D$_{in}$) and are classified as type I½ inhibitors. LY3009120 and lifirafenib, which are in the early drug-development stage, bind to a different inactive form of B-Raf (DFG-D$_{out}$) and are classified as type II inhibitors. Besides targeting B-Raf and MEK protein kinases, immunotherapies that include ipilimumab, pembrolizumab, and nivolumab have been FDA-approved for the treatment of melanomas. Current clinical trials are underway to determine the optimal usage of targeted and immunotherapies.

1. The Ras-Raf-MEK-ERK (MAP kinase) signaling pathway

Protein kinases play pivotal roles in nearly every aspect of cell physiology [1–3]. They regulate cell growth, cell division, cell migration, metabolism, nervous system function, the immune response, and transcription. Because regulatory protein phosphorylation involves the action of both protein kinases and phosphoprotein phosphatases, phosphorylation-dephosphorylation is an overall reversible process. Dysregulation of protein kinase signaling occurs in many diseases including cancer, diabetes, and inflammatory disorders. Protein kinases catalyze the following reaction:

Abbreviations: AS, activation segment; CRD, cysteine-rich domain; CS or C-spine, catalytic spine; CL, catalytic loop; CTT, carboxyterminal tail; EGFR, epidermal growth factor receptor; HGF, hepatocyte growth factor; GK, gatekeeper; GRL, Gly-rich loop; KSR, kinase suppressor of Ras; NSCLC, non-small cell lung cancer; PDGFR, platelet-derived growth factor receptor; PKA, protein kinase A; pY or pTyr, phosphotyrosine; RS or R-spine, regulatory spine; Sh2, shell residue 2; VEGFR, vascular endothelial growth factor receptor

E-mail address: rrj@brimr.org.

https://doi.org/10.1016/j.phrs.2018.08.013
Received 9 August 2018; Accepted 13 August 2018
Available online 15 August 2018

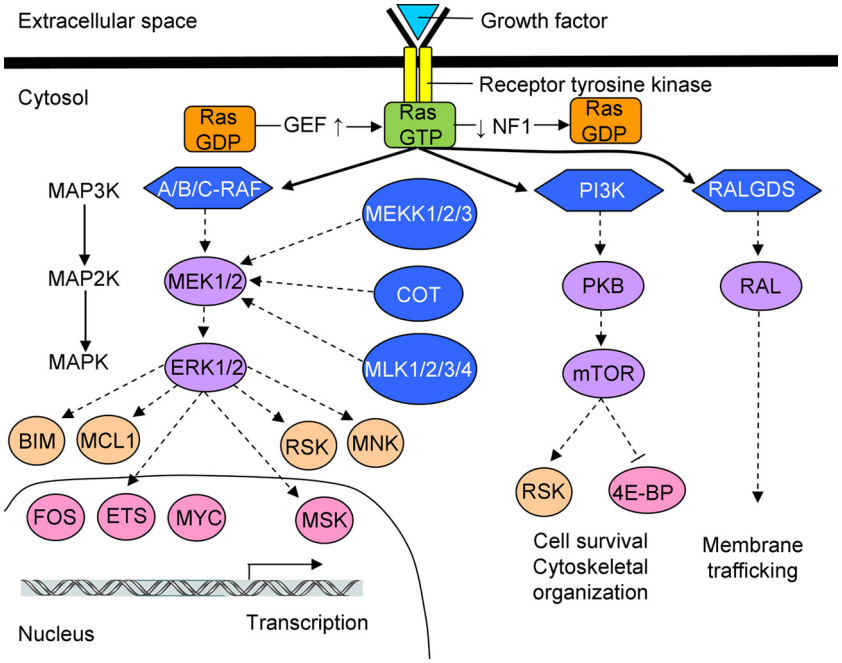

Fig. 1. Ras effector modules including the evolutionarily conserved MAP kinase Ras-Raf-MEK-ERK pathway. GEF action increases the level of Ras-GTP and NF1 activity decreases the level of Ras-GTP. The dashed lines indicate that several steps may be involved. GEF, guanine nucleotide exchange factor; NF1, neurofibromin-1.

$$MgATP^{1-} + protein\text{–}O{:}H \rightarrow protein\text{–}O{:}PO_3^{2-} + MgADP + H^+$$

Note that the phosphorylium ion (PO_3^{2-}), and not the phosphate group (OPO_3^{2-}), is transferred from ATP to the protein substrate. Based upon the nature of the phosphorylated −OH group, these enzymes are classified as protein-serine/threonine or protein-tyrosine kinases [4]. A small group of dual-specificity protein kinases such as MEK1/2 catalyzes the phosphorylation of ERK1/2 at tyrosine before threonine in the ERK activation segment sequence Thr-Glu-Tyr [5,6]. These dual-specificity protein catalysts are members of the protein-serine/threonine kinase family.

The Ras-Raf-MEK-ERK signal transduction cascade is arguably the most important oncogenic pathway in human cancers [7–11]. This highly conserved pathway transmits signals from extracellular growth factors and cytokines into intracellular signaling modules. The mitogen-activated protein kinase (MAP kinase) cascade is triggered by a variety of transmembrane receptors. Activated receptor protein-tyrosine kinases such as epidermal growth factor receptor (EGFR) become phosphorylated at tyrosine residues and these phosphorylated sites attract various adapter proteins and guanine nucleotide exchange factors (GEFs) such as SOS (from *Drosophila* son of sevenless). The GEFs mediate the transformation of inactive Ras-GDP to active Ras-GTP within the inner leaflet of the plasma membrane [7–9]. Of importance, essentially all of Ras biochemistry and signaling occurs within the plasma membrane. The *RAS* (Rat sarcoma) gene family consists of three members: *KRAS* (Kirsten rat sarcoma viral oncogene homolog), *HRAS* (Harvey rat sarcoma viral oncogene homolog), and *NRAS* (neuroblastoma RAS viral (v-ras) oncogene homolog). These proteins toggle between inactive and active forms; the conversion of inactive Ras-GDP to active Ras-GTP turns the switch on while intrinsic Ras-GTPase activity stimulated by the GTPase activating proteins (GAPs) such as NF1 (neurofibromin-1) turns the switch off.

The molecular weights of H-Ras, K-Ras, and N-Ras are about 21 kDa. In contrast, GEFs and GAPs are large (150–300 kDa) multi-domain proteins capable of an astounding variety of interactions with other proteins, lipids, and regulatory molecules that control levels of active and inactive Ras [9]. To activate downstream components of the MAP kinase pathway, Ras-GTP stimulates the formation of active homodimers or heterodimers of A-Raf, B-Raf, and C-Raf by an intricate process (the Raf acronym corresponds to Rapidly accelerated fibrosarcoma, first described in mice). A-Raf, B-Raf, and C-Raf are protein-serine/threonine protein kinases that catalyze the phosphorylation and activation of MEK1 and MEK2 where MEK corresponds to MAP/ERK Kinase. MEK1 and MEK2, in turn, catalyze the phosphorylation and activation of ERK (Extracellular signal-Regulated protein Kinase).

The Raf enzymes and MEK1/2 have very narrow substrate specificity [5,6]. Accordingly, the only known substrates of the Raf enzymes are MEK1/2 and the only known substrates of MEK1/2 are ERK1/2. To further exemplify their dedicated substrate specificity, MEK1/2 are unable to catalyze the phosphorylation of denatured ERK1/2 nor do they catalyze the phosphorylation of peptides with the sequence corresponding to the activation segment of ERK1/2, the physiological substrate. In contrast to the Raf and MEK enzymes, ERK1 and ERK2 have broad substrate specificity and they can catalyze the phosphorylation of hundreds of different proteins [11]. The Kinase Suppressor of Ras protein kinases (KSR1/2) are the closest relatives of the Raf family kinases [4]. KSR1/2 are impaired protein kinases (but not kinase dead) that function as scaffolds to assemble Raf, MEK, and ERK to increase signaling efficiency [11]. The effect of KSR1/2 is context-dependent and varies with the concentration of the various components of the MAP kinase pathway; accordingly, these proteins can be stimulatory or inhibitory.

The MAP kinase cascade consists of a tier of three protein kinases: (i) MAPK kinase kinase (MAP3K), (ii) MAPK kinase (MAP2K), and (iii) and MAPK. Although A/B/C-Raf are at the proximal end of the MAP kinase cascade, COT (also known as cancer Osaka thyroid kinase or MAP3K8), MEKK1/2/3, and MLK1/2/3/4 are other ERK1/2 MAP3Ks that participate in specialized cell type and stimulation specific responses (Fig. 1) [13]. Ras-GTP has additional downstream effector pathways including the phosphatidylinositol 3-kinase (PI3 kinase), the Ral-GDS, as well as the MAP kinase modules [12,14,15]. Akt/PKB is downstream from PI3 kinase. This suggests the strategy of combining targeted inhibitors of Raf and MEK1/2 of the MAP kinase pathway along with inhibition of PI3 kinase and Akt/PKB in the treatment of various neoplasms.

2. Activation of the Ras-MAP kinase pathway in human malignancies including melanomas

RAS mutations occur in about 30% of all cancers [16]. *KRAS* mutations occur in about 70% of pancreatic ductal adenocarcinomas, 40% of colorectal cancers, 20% of papillary thyroid cancers, 10% of acute myelogenous and acute lymphoblastic leukemias, 35% of non-small cell lung cancers (NSCLC), and 10% of breast and ovarian cancers [17]. Moreover, *NRAS* mutations occur in about 15% of anaplastic thyroid cancers and follicular thyroid cancers and 20% of malignant melanomas; mutations of *HRAS* occur in about 20% of urothelial bladder and 2% of renal cell carcinomas [17]. Although investigators have tried to develop Ras inhibitors for decades, it is only recently that there has been a modicum of success [18–22]. However, no inhibitors of Ras *per se* have yet entered clinical trials. As an alternative, combinations of Raf and MEK inhibitors that target the MAP kinase pathway have been developed. So far, these inhibitors have been approved for the treatment of advanced melanoma with activating mutations in *BRAF*; the term advanced in the oncology setting usually means unresectable and/or metastatic.

Mutational activation of the Ras-Raf-MEK-ERK pathway occurs in more than 90% of skin melanomas [23,24]. The Cancer Network consortium examined the genetic background of cutaneous melanomas in 331 patients based upon DNA, RNA, and protein analysis [24]. They found that the incidence of *BRAF* mutations was 52%, that of *NRAS* mutations was 28%, and that of *NF1* mutations was 14%; they classified the balance of cases as Triple-WT (wild type). The gain-of-function *BRAF* and *NRAS* mutations and the loss-of-function *NF1* mutations activate the MAP kinase pathway. In addition to melanoma, *BRAF* mutations occur in other cancers. Such mutations occur in 10–70% of thyroid cancers (depending upon the histology), about 10% of colorectal cancers, and 3–5% of NSCLC [25–28].

The finding that activating *BRAF* mutations occur in the majority of melanomas [29] prompted the pursuit of B-Raf inhibitors [30]. Sorafenib was initially developed as a C-Raf kinase inhibitor (reflected in its name sorafenib). However, sorafenib is a multikinase inhibitor with actions against Flt3, Kit, and VEGFR1/2/3. Numerous clinical trials of sorafenib were performed in patients with advanced or metastatic melanoma. Eisen et al. reported that sorafenib produced favorable clinical responses in fewer than 5% of patients with melanoma [31]. Its activity against B-Raf (wild type and V600E mutants) is less than that against C-Raf, which explains in part the lack of efficacy in the treatment of melanoma patients. It is currently FDA-approved for the treatment of liver, renal cell, and differentiated thyroid carcinomas (www.brimr.org/PKI/PKIs.htm). In contrast, Chapman et al. described a clinical trial that compared vemurafenib (also known as PLX4032) with dacarbazine (a cytotoxic DNA-alkylating agent) in a total of 675 randomized melanoma patients with the $BRAF^{V600E}$ mutation [32]. They found that the response rate for vemurafenib was 48% while that for dacarbazine was 5%. Adverse side effects of vemurafenib included arthralgia (joint pain), diarrhea, fatigue, nausea, and skin rash along with the generation of keratoacanthomas, which are well-differentiated squamous cell skin carcinomas. These tumors are readily identified, simple to excise, and not metastatic. However, the development of such tumors is clearly an undesired outcome. Fatigue, rash, and diarrhea are adverse events that occur with nearly all small molecule protein kinase inhibitors [33]. Vemurafenib was FDA-approved for the treatment of $BRAF^{V600E}$ melanomas in 2011.

Dabrafenib was the second B-Raf inhibitor to enter clinical trials in comparison with dacarbazine. Hauschild et al. observed that the overall response rate for dabrafenib was 50% while that for dacarbazine was 6% [34]. Dabrafenib produced a progression-free survival of 5.1 months compared with 2.7 months for dacarbazine. Adverse events were similar to those of vemurafenib. However, dabrafenib is prone to cause fever [34] while vemurafenib is associated with photosensitivity [32]. Dabrafenib was FDA-approved for the treatment of patients with advanced melanomas with the $BRAF^{V660E}$ mutation in 2013 (www.brimr.org/PKI/PKIs.htm). As described for vemurafenib, about 20% of patients receiving dabrafenib develop keratoacanthomas. These disorders are treated by surgical excision and these drugs can be continued without dose adjustments. However, both of these drugs are ineffective in the treatment of patients lacking the $BRAF^{V600E}$ mutation.

Vemurafenib and dabrafenib produce the paradoxical activation of the MAP kinase pathway in wild type *BRAF* cells [5,11]. It is paradoxical in the sense that a B-Raf antagonist results in the activation of the pathway. This paradoxical activation leads to drug-induced skin lesions (keratoacanthomas and squamous cell carcinomas) as noted above. Owing to this paradoxical activation, both vemurafenib and dabrafenib promote growth and metastasis of tumor cells bearing *RAS* mutations in animal studies and are contraindicated for the treatment of cancer patients with wild type *BRAF*, including patients with activating *RAS* mutations. The exact mechanism of paradoxical activation is unclear despite extensive experimentation, but drug-induced Raf dimerization appears to be an essential step. In one scheme, it is hypothesized that a B-Raf inhibitor triggers the formation of a Ras-dependent B-Raf–C-Raf heterodimer. Activation then follows when the B-Raf inhibitor is not able to effectively inhibit both protomers of the dimer, leaving the unoccupied C-Raf protomer activated and allowing ATP binding and catalytic activity. In a second scheme Raf activation is the result of transactivation. Drug binding to one member of the Raf homodimer or heterodimer inhibits one partner but results in the transactivation of the second drug-free partner as a result of a conformational change. Thus, effective inhibition of the transactivated partner is necessary for abrogating the paradoxical activation. According to either scheme, a pan-Raf inhibitor with true cellular activities against all Raf isoforms is thought to be essential for minimizing paradoxical activation. In order to eliminate the drawbacks associated with paradoxical MAP kinase pathway activation and to provide therapeutic benefit to people with *RAS* mutant cancers, it will be necessary to identify drugs that are potent inhibitors of $B\text{-}Raf^{V600E}$, B-Raf, and C-Raf.

Although the majority of people with advanced melanoma with the $BRAF^{V600E}$ mutation derive clinical benefit, median progression-free survival is only six months and 90% of patients develop resistance within one year [33]. This rapid development of secondary resistance has prompted the exploration of other inhibitors of the MAP kinase pathway. One of these was trametinib, which is a potent inhibitor of MEK1/2. In a clinical trial with 322 advanced melanoma patients possessing $BRAF^{V600E/K}$ mutations, Flaherty et al. discovered that trametinib resulted in an improved overall response rate (22% vs. 8%) and progression-free survival (4.8 vs. 1.5 months) when compared with groups receiving cytotoxic dacarbazine or paclitaxel [35]. Peripheral edema, rash, and diarrhea were the principal trametinib adverse events, which were easily managed. Mild grade 1/2 ocular toxicity (blurred vision) occurred in 9% of the patients most likely resulting from serous retinopathy, a reversible disorder. In contrast to vemurafenib and dabrafenib therapy, these trametinib patients did not develop secondary skin neoplasms.

In a clinical trial with 97 patients, Kim et al. found significant clinical activity with trametinib in B-Raf-inhibitor–naive patients that were previously treated with chemotherapy, immunotherapy, or both [36]. However, they found minimal clinical activity with trametinib as a second-line treatment in patients who were previously treated with a B-Raf inhibitor. These investigators suggested that B-Raf-inhibitor resistance mechanisms also confer resistance to MEK-inhibitor monotherapy. Accordingly, the FDA approved trametinib initially (2013) for the treatment of patients who had not received targeted B-Raf inhibitor therapy (www.brimr.org/PKI/PKIs.htm).

In a clinical trial involving 247 patients with advanced melanoma with $BRAF^{V600}$ mutations, Flaherty et al. compared trametinib and dabrafenib monotherapy with the combination of these two drugs [37]. They observed that the frequency of complete or partial responses was

Table 1
Selected FDA-approved therapies for advance melanomas[a].

Agent	Mechanism	Indications
Targeted therapies		
Vemurafenib	B-Raf$^{V600E/K}$ inhibitor	As monotherapy or in combination with cobimetinib for *BRAF*$^{V600E/K}$-mutant disease
Dabrafenib	B-Raf$^{V600E/K}$ inhibitor	As monotherapy or in combination with trametinib for *BRAF*$^{V600E/K}$-mutant disease
Encorafenib	B-Raf$^{V600E/K}$ inhibitor	In combination with binimetinib for *BRAF*$^{V600E/K}$-mutant disease
Trametinib	MEK1/2 inhibitor	As monotherapy or in combination with dabrafenib for *BRAF*$^{V600E/K}$-mutant disease
Cobimetinib	MEK1/2 inhibitor	In combination with vemurafenib for *BRAF*$^{V600E/K}$-mutant disease
Binimetinib	MEK1/2 inhibitor	In combination with encorafenib for *BRAF*$^{V600E/K}$-mutant disease
Immunotherapies		
Ipilimumab	Anti-CTLA-4 antibody[b]	As monotherapy or in combination with nivolumab
Pembrolizumab	Anti-PD-1 antibody[c]	As monotherapy
Nivolumab	Anti-PD-1 antibody[c]	As monotherapy or in combination with ipilimumab

[a] Data from Ref. [42].
[b] CTLA-4, cytotoxic T-lymphocyte-associated antigen 4.
[c] PD-1 programmed cell death protein-1.

76% for the combination group while it was 54% for monotherapy groups. Moreover, median progression-free survival was 9.4 months for the combination therapy group while it was 5.8 months for the monotherapy groups. Pyrexia, or fever, was much more common in the combination cohort when compared with the monotherapy groups (71% vs. 26%). The occurrence of hyperkeratosis (9% vs. 30%) and cutaneous squamous cell carcinomas (7% vs. 19%) was decreased in the combination therapy cohort when compared with the monotherapy group; however, these results did not achieve statistical significance ($P = 0.09$). The protective effect of dual therapy may be due to the MEK inhibitor blockade of the paradoxical activation of the MAP kinase pathway produced by dabrafenib. The combination of dabrafenib and trametinib was approved by the FDA for the treatment of *BRAF*$^{V600E/K}$ in 2014 (www.brimr.org/PKI/PKIs.htm).

Larkin et al. reported on the findings of a clinical trial consisting of 495 patients with previously untreated advanced *BRAF*^{V600}-mutation positive melanoma receiving both vemurafenib and cobimetanib or vemurafenib plus placebo (the control group) [38]. The frequency of complete or partial responses (68% vs. 45%) and the duration of median progression-free survival (9.9 vs. 6.2 months) was better in the dual-therapy cohort when compared with the control group. The incidence of keratoacanthomas was 1% in the combination group compared with 8% in the vemurafenib-only group while the incidence of cutaneous squamous cell carcinomas in the combination group was 2% compared with 11% in the control group. This represents an unusual situation where a combination therapy produced fewer adverse events than a monotherapy [33]. The studies of Larkin et al. [38] and Flaherty et al [37] indicate that the use of the combination of the B-Raf and MEK1/2 inhibitors is more effective than that of B-Raf or MEK1/2 inhibitor monotherapy.

Dummer et al. reported on the findings of a clinical trial consisting of 577 patients with advanced *BRAF*^{V600}-mutation positive melanoma that was previously untreated or that had progressed on or after first-line immunotherapy [39]. Patients were randomly assigned to receive either oral encorafenib once daily plus oral binimetinib twice daily (encorafenib plus binimetinib cohort), oral encorafenib once daily (encorafenib cohort), or oral vemurafenib twice daily (vemurafenib cohort). With a median follow-up of 16.6 months, median progression-free survival was 14.9 months in the encorafenib plus binimetinib cohort and 7.3 months in the vemurafenib cohort. The overall response rate was 63%. The most common grade 3–4 adverse events seen in the encorafenib plus binimetinib group were increased γ-glutamyl-transferase activity (a liver enzyme) in 9% of patients, increased creatine phosphokinase (chiefly a muscle enzyme) in 7% of patients, and hypertension in 6% of patients. These investigators concluded that encorafenib plus binimetinib and encorafenib monotherapy showed favorable efficacy compared with vemurafenib. Moreover, they concluded that encorafenib plus binimetinib appears to have an improved tolerability profile compared with encorafenib or vemurafenib. As a consequence of these findings, the FDA approved the combination of encorafenib and binimetinib for the treatment of *BRAF*$^{V600E/K}$-positive advanced melanoma in 2018 (www.brimr.org/PKI/PKIs.htm).

The FDA has approved three B-Raf and MEK1/2 inhibitor combinations for the treatment of patients with advanced melanomas that possess a *BRAF*^{V600} mutation (about 50% of all advanced melanoma patients): (i) vemurafenib and cobimetanib, (ii) dabrafenib and trametinib, and (iii) encorafenib and binimetinib. The use of drug combinations is now the standard of care for such patients [40]. It is unclear whether any of these drug combinations is superior to the others. The choice between dabrafenib and trametinib versus vemurafenib and cobimetanib may depend upon patient-related factors; in the former case, it is the ability to tolerate fever and in the latter case it is the ability to tolerate cutaneous side effects. However, encorafenib–binimetinib seems to have the most attractive toxicity profile, with a much lower frequency of fever and photosensitivity in patients when compared with other two B-Raf–MEK inhibitor combinations [39]. Perhaps differences in overall survival will be observed as these studies are continued. The addition of a MEK inhibitor to a B-Raf inhibitor allows for a greater therapeutic dosage of the latter and increases overall effectiveness.

In addition to targeted therapies, the use of parenterally administered immune checkpoint therapies has emerged in the effective treatment of melanomas [41,42]. Ipilimumab is a monoclonal antibody that activates the immune response by targeting cytotoxic T-lymphocyte antigen-4 (CTLA-4), which is a protein that down regulates the immune response. Pembrolizumab is a humanized monoclonal antibody that activates the immune response by targeting the programmed cell death-1 (PD-1) receptor. Nivolumab, which is a human IgG4 anti-PD-1 monoclonal antibody, is another checkpoint inhibitor. All three of these immune checkpoint inhibitors are FDA-approved for the treatment of advanced melanomas regardless of *BRAF* mutation status (Table 1). For patients with documented *BRAF*^{V600} mutations, selection between immune checkpoint therapy and targeted therapy is currently problematic owing to the lack of results from ongoing clinical trials comparing the two approaches. The studies documented in this section show that significant strides have been made in the past seven years in the treatment of metastatic melanomas and additional studies are underway that may add to the effectiveness of both targeted and immune checkpoint modalities. Another possibility to improve clinical outcomes is to combine immune checkpoint and targeted therapies. Some of the initial clinical trials combining targeted and immunotherapy were unsuccessful owing to toxicities, but subsequent trials using different protocols are in progress. Moreover, targeted and immunotherapies might be combined together or given sequentially. The outcomes of immunotherapy (ipilimumab and nivolumab) followed by B-Raf targeted therapy (dabrafenib and trametinib), or *vice versa*, are being

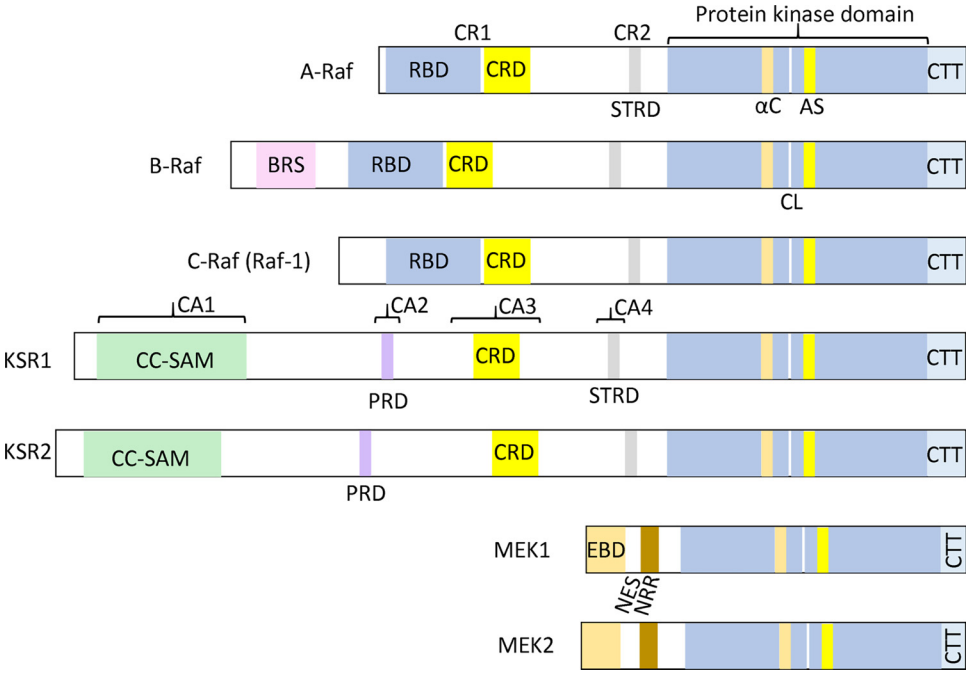

Fig. 2. Architecture of A/B/C-Raf, KSR1/2, and MEK1/2. AS, activation segment; BRS, B-Raf specific sequence; CL, catalytic loop; CR, conserved region; CRD, cysteine-rich domain; CC-SAM, coiled-coil and sterile-α-motif; CTT carboxyterminal tail; EBD, ERK-binding domain; NES, nuclear export sequence; NRR, negative regulatory region; PRD, proline-rich domain; RBD, Ras-binding domain; STRD, serine-threonine rich domain.

compared in an ongoing clinical trial (NCT02224781).

3. Properties of the Raf protein-serine/threonine kinases and KSR1/2

3.1. Primary, secondary, and tertiary structures of the Raf family kinases and KSR1/2

As noted in Section 1, the Raf family consists of three enzymes: A-, B-, and C-Raf while KSR1 and KSR2 are the closest relatives of the Raf family. Each of the Raf proteins shares three conserved regions (CR) appropriately named CR1, CR2, and CR3. CR1 consists of a Ras-binding domain (RBD) followed by a cysteine-rich domain (CRD). CR1 interacts with Ras and with membrane phospholipids during Raf activation. CR2 is a serine-threonine rich segment that is able to bind to the regulatory protein 14-3-3 following the phosphorylation of specific serine residues (S214/S365/S259 in A/B/C-Raf, respectively) [5]. The 14-3-3 protein bound at these sites is inhibitory; dephosphorylation of these phosphoserine residues is required for enzyme activation. CR3 is the protein kinase domain that is followed by a carboxyterminal tail (CTT) (Fig. 2). CTT contains a serine residue that, when phosphorylated, is able to bind an activating14-3-3 protein (S582/S729/S621 in A/B/C-Raf, respectively). The BRS (B-Raf specific) domain is N-terminal to CR1; it mediates the interaction between it and the KSR proteins [43].

KSR1 and KSR2 contain five conserved domains (CA1–CA5). The amino termini of KSR1 and KSR2 contain a CA1 segment that contributes to their binding to B-Raf (Fig. 2) [44]. A coiled-coil and sterile-α-motif (CC-SAM) within this region contribute to membrane binding. CA2 is a proline-rich segment of unknown function. CA3 is a cysteine-rich segment that contributes to membrane localization through its binding to phospholipids; it is similar to the CRD of the Raf family. CA4 is a serine/threonine rich segment that contributes to ERK1/2 binding, a process that requires active Ras. CA4 is similar to the CR2 region of the Raf family and CA5 corresponds to the protein kinase domain.

The catalytic domain of each of the human Raf family kinases consists of 261 amino acid residues, which is about the average size of a protein kinase lacking any inserts. Based upon the primary structures of about five dozen protein-tyrosine and protein-serine/threonine kinases, Hanks and Hunter subdivided protein kinases into 12 domains (I-VIA, VIB-XI) [45]. Domain I of protein kinases contains a glycine-rich loop (GRL) with a GxGxΦG signature, where Φ refers to a hydrophobic residue and is phenylalanine in the case of the Raf enzymes. The glycine-rich loop connects the β1- and β2-strands that make up a portion of the roof of the ATP/ADP-binding site. The flexible glycine-rich loop allows for both ATP binding and ADP release during each catalytic cycle. Domain II of the Raf enzymes contains a conserved Ala-Xxx-Lys (AVK) sequence in the β3-strand and Hanks domain III contains a conserved glutamate in the αC-helix (B-Raf E501) that forms a salt bridge with the conserved β3-lysine (B-Raf K483) in all active protein kinases (Fig. 3A) as well as many dormant protein kinase conformations (Fig. 3C). Domain V of the Raf enzymes contains a QWCEG hinge that connects the small and large lobes.

Domain VIB within the large lobe of the Raf enzymes contains a conserved HRD sequence, which forms part of the catalytic loop HRD $(x)_4N$ (Table 2). Domain VII of the Raf enzymes contains a DFG signature and domain VIII of B/C-Raf contains an APE sequence while that of A-Raf contains an AAE sequence; the DFG is the beginning of the Raf activation segment while the AxE corresponds to its end. These 30-residue segments exhibit different conformations in the active and inactive states. Domains IX–XI make up the αE–αI helices (Fig. 3A/C/E). The X-ray crystallographic structure of the catalytic subunit of murine protein kinase A (PKA) produced an invaluable blueprint for formulating the roles of the 12 Hanks domains and the structure has shed light on the underlying biochemistry of the entire protein kinase superfamily (PDB ID: 2CPK) [46,47]. All protein kinases possess a small amino-terminal and a large carboxyterminal lobe that are connected by the hinge segment [1]. The amino-terminal lobe of all protein kinases contains five β-strands (β1–5) and an important regulatory αC-helix and the carboxyterminal lobe of active enzymes contains seven conserved helices (αD–αI and αEF) along with four β-strands (β6–β9) (Fig. 3A). Of the hundreds of protein kinase structures that have been reported, all of these enzymes contain the protein kinase fold as first described for PKA [1,46,47].

All active protein kinases possess a K/E/D/D (Lys/Glu/Asp/Asp) amino acid signature that is required for catalysis (Table 2) [1]. The lysine and glutamate occur within the amino-terminal lobe and the two aspartate residues occur within the carboxyterminal lobe. ATP binds next to the hinge within the cleft between the two lobes and interacts with each lobe. Comprehensive analyses indicate that a salt bridge between the β3-lysine and the αC-glutamate is required for the

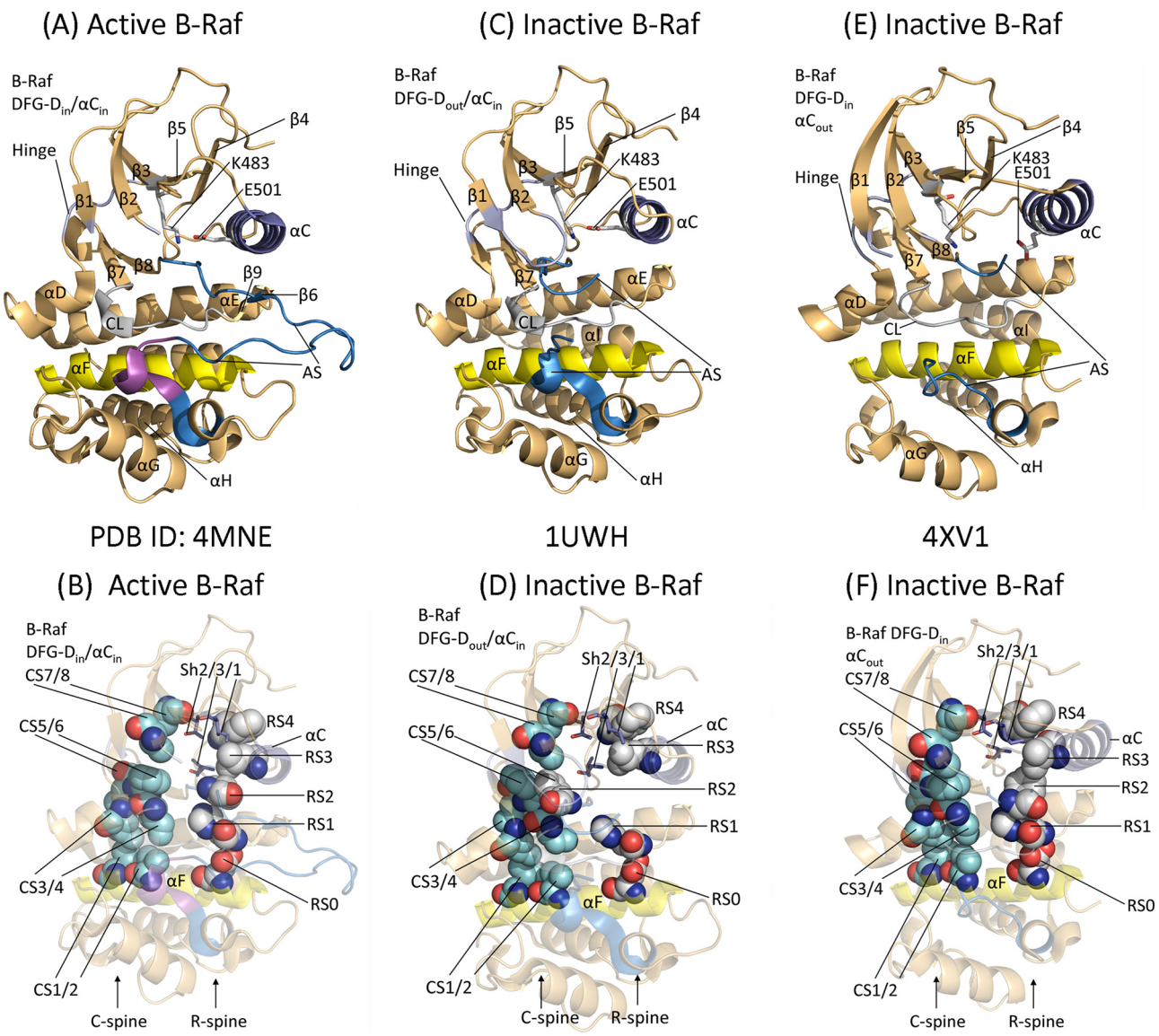

Fig. 3. (A) and (B) Active B-Raf; PDB ID: 4MNE (C) and (D) Inactive B-Raf with αC$_{in}$ and DFG-D$_{out}$; PDB ID: 1UWH (E) and (F) Inactive B-Raf with αC$_{out}$ and DFG-D$_{in}$; PDB ID: 4XV1. AS, activation segment; CL, catalytic loop; CS, catalytic spine; RS, regulatory spine. All figures except for 1, 2, and 9 were prepared using the PyMOL Molecular Graphics System Version 1.5.0.4 Schrödinger, LLC.

formation of an active protein kinase conformation, which corresponds to an "αC$_{in}$" arrangement as shown for active B-Raf (Fig. 3A). These residues in many inactive enzymes fail to form this salt bridge and thereby form an inactive "αC$_{out}$" structure (See Ref. [1] for details). The αC$_{in}$ conformation is necessary, but not sufficient, for the expression of catalytic activity. Although the β3-K483 and αC-E501 of dormant B-Raf form a salt bridge (Fig. 3C), molecular measurements show that this corresponds to an αC-dilated structure as described later in this Section. Moreover, the activation segment of B-Raf with the αC-dilated structure has an inactive DFG-D$_{out}$ conformation that blocks ATP and protein substrate binding.

The large carboxyterminal lobe contains catalytic loop residues within domain VIb that play essential structural and catalytic roles. Additionally, two Mg^{2+} ions participate in each catalytic cycle of several protein kinases [48–50] and two Mg^{2+} ions are presumably required for the proper functioning of the Raf enzymes. By inference, the DFG-D594 (the second D of K/E/D/D) binds to Mg^{2+}(1), which in turn binds to the β- and γ-phosphates of ATP. The asparagine at the end of the catalytic loop (HRD(x)$_4$N) binds to Mg^{2+}(2). Mg^{2+}(2) is bound to the enzyme with high affinity while Mg^{2+}(1) binds with lower affinity. The two Mg^{2+} ions neutralize the negative charges of the phosphate groups. While Mg^{2+}(1) appears to be critical for the phosphoryl transfer, Mg^{2+}(2) binds first as a complex with ATP [50]. In the active conformation, the DFG-D is directed inward toward the active site where it can bind Mg^{2+}(1) as depicted in Fig. 4A. In contrast, the DFG-D of inactive B-Raf is pointed outward producing an inactive DFG-D$_{out}$ structure (Fig. 4B).

The relative location of the β3-strand and αC-helix is an important structural parameter and this has led to the DFG-D$_{in}$ and DFG-D$_{out}$ classification. Additionally, Vijayan et al. examined the structures of about 200 hundred protein kinases and they divided the DFG-D$_{out}$ structures into (i) classical and (ii) nonclassical groups [51]. This division was necessary owing to the differences in the location of the activation segment DFG-D and DFG-F in the eukaryotic kinome. They described two measurements that differentiated between the classical and nonclassical DFG-D$_{out}$ groups and named them D1 and D2. D1 is the distance between the αC-atom of the HRD(x)$_4$N-asparagine at the end of the catalytic loop and of the DFG-F of the activation segment and D2 is the distance between the αC-atom of the αC-E residue and the DFG-F. The protein kinase exhibits a classical DFG-D$_{out}$ structure provided that

Table 2
Important human (i) Raf family, (ii) KSR1/2, and (iii) MEK1/2 residues[a].

	A-Raf	B-Raf	C-Raf	KSR1	KSR2	MEK1	MEK2	Inferred function
No. of amino acids →	606	766	648	921	950	392	400	
Component ↓								
CC-SAM				(CA1) 31–171	(CA1) 20–154			
PRD	None	None	None	(CA2) 271–292	(CA2) 273–293			
RBD	19–91	155–227	56–131	None	None			
CRD	98–144	234–280	138–184	(CA3) 347–391	(CA3) 412–456			
S/T-RD	257–269	363–373	212–224	(CA4) 444–458	(CA4) 517–531			
CR1	14–154	150–290	51–194					
CR2	209–224	360–375	254–269					
Protein kinase domain	310–570	457–717	349–609	613–883	666–931	68–361	72–369	Catalyzes substrate phosphorylation
Glycine-rich loop	^{317}GTGSFG^{322}	^{464}GSGSFG^{469}	^{356}GSGSFG^{361}	^{620}GQGRWG^{625}	^{673}GKGRFG^{678}	^{75}GAGNGG^{80}	^{79}GAGNGG^{84}	Anchors ATP β-phosphate
β3-K or R of K-R/E/D/D	K336	K483	K375	R637	R692	K97	K101	Forms salt bridges with ATP α- and β-phosphates and with αC-E
αC-E, E of K/E/D/D	E354	E501	E393	E650	E710	E114	E118	Forms salt bridges with β3-K
Hinge	^{383}QWCEG^{387}	^{530}QWCEG^{534}	^{422}QWCEG^{426}	^{687}SFCKG^{691}	^{740}SLCKG^{745}	^{144}EAMDG^{148}	^{148}EHMDG^{152}	Connects N- and C-lobes
Catalytic loop	^{427}HRDLKSNN^{434}	^{574}HRDLKSNN^{581}	^{466}HRDMKSNN^{473}	^{729}HKDLKSKN^{736}	^{784}HKDLKSKN^{791}	^{188}HRDVKPSN^{192}	^{192}HRDVKPSN^{199}	Plays both structural and catalytic functions
Catalytic loop HRD-D, First D of K/E/D/D	D429	D576	D468	D731	D786	D190	D194	Catalytic base
Catalytic loop Asn	N434	N581	N473	N736	N791	N193	N199	Chelates Mg^{2+}(2)
AS DFG-D, Second D of K/E/D/D	D447	D594	D486	D748	D803	D208	D212	Chelates Mg^{2+}(1)
End of AS	^{474}AAE^{476}	^{621}APE^{623}	^{513}APE^{515}	^{778}APE^{780}	^{833}APE^{835}	^{231}SPE^{233}	^{235}APE^{237}	Interacts with the αHI loop and stabilizes the AS
AS phosphorylation sites	T452, T455	T599, S602	T491, S494	S755, S770	S808, S810	S218, S222	S222, S226	Stabilizes the AS after phosphorylation
C-terminal tail	571–606	718–766	610–648	884–921	932–950	362–392	370–400	Signal transduction
C-terminal tail phosphorylation sites	S582	S729/750/753	S621/642	S888	None	None	T394/T396	
MW (kDa)	67.6	84.4	73.1	102	108	43.4	44.4	
UniProtKB accession no.	P10398	P15056	P04049	Q8IVT5	Q6VAB6	Q02750	P36507	

[a] AS, activation segment; CC-SAM, coiled-coil and sterile-α-motif; CR1, conserved region-1; CRD, cysteine-rich domain; PRD, proline-rich domain; RBD, Ras-binding domain; S/T RD serine/threonine-rich domain.

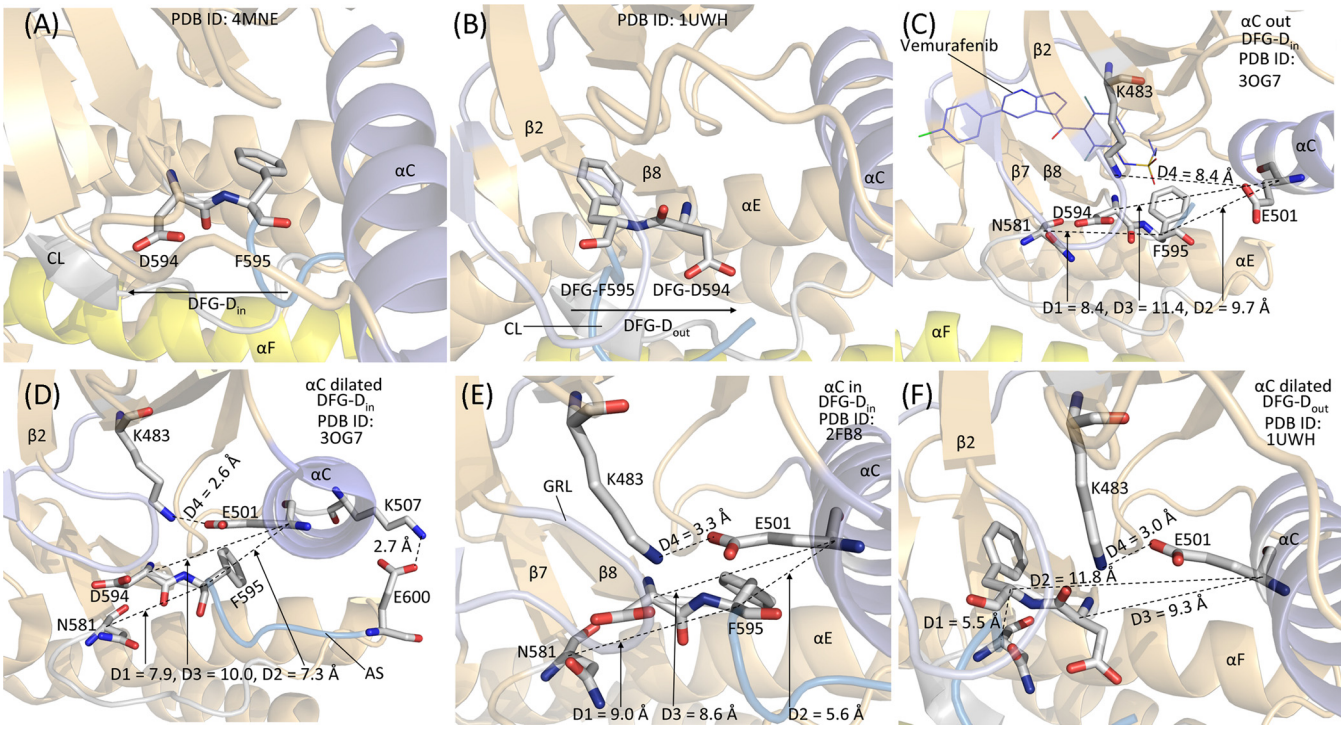

Fig. 4. (A) DFG-D_{in} structure. (B) DFG-D_{out} structure. (C—F) D1/2/3/4 measurements. D1 is the distance between the α-carbon atom of the terminal asparagine of the catalytic loop and the α-carbon atom of DFG-F; D2 is the distance from the α-carbon atom of the αC-E and that of DFG-F; D3 is the distance from the α-carbon atom of the αC-E and DFG-D; D4 is the distance from the ε-amino group of β3-K and the carboxyl group of αC-E.

D2 is greater than 9 Å; classical DFG-D_{out} structures have long Phe/Glu distances (D2 ≥ 9.0 Å) and short Phe/Asn distances (D1 ≤ 7.2 Å).

The D2 value in the structure of dormant αC_{out}/DFG-D_{in} B-Raf (PDB ID: 3OG7, bound to vemurafenib) equals 9.7 Å (Fig. 4C); accordingly, this is within the classical DFG-D_{out} group. These investigators measured the distance from the α-carbon atom of αC-E and DFG-D, which we named D3, and found that a D3 measurement of less than 9 Å represents the αC_{in} structure while those with a D3 measurement greater than 10.5 Å represent an αC_{out} configuration while values within this range were classified as αC-dilated. The structure of inactive αC-dilated/DFG-D_{in} B-Raf (PDB ID: 3OG7, free protomer) has a D3 value of 10.0 Å (Fig. 4D), which corresponds to the αC-dilated classification. The structure of active αC_{in}/DFG-D_{in} B-Raf (PDB ID: 2FB8) has D1, D2, and D3 values of 9.0 Å, 5.6 Å, and 8.6 Å, respectively; these values are consistent with an active αC_{in}/DFG-D_{in} classification (Fig. 4E). The structure of inactive αC-dilated/DFG-D_{out} has D1, D2, and D3 values of 5.5 Å, 11.8 Å, and 9.3 Å, respectively (Fig. 4F). Its D2 value is greater than 9 Å indicative of an DFG-D_{out} structure and its D3 value falls between 9 Å and 10.5 Å indicative of an αC-dilated structure. The electrostatic bond between β3-K483 and αC-E501 is broken in the inactive B-Raf αC_{out} configuration. However, Vijayan et al. reported that this salt bridge occurs in ≈ 90% of DFG-D_{out} structures and they call these αC-dilated structures to differentiate them from αC_{in} configurations [51]. The distance between the β3-lysine ε-amino group and αC-glutamate carboxyl group, which we called D4, is 3.3 Å in the αC_{in}/DFG-D_{in} structure (PDB ID: 2FB8), 2.6 Å in the αC-dilated/DFG-D_{in} structure (3OG7), 8.4 Å in the αC_{out} /DFG-D_{in} structure (3OG7), and 3.0 Å in the αC-dilated/DFG-D_{out} structure.

The protein kinase activation segment, which is typically 20–30 residues in length with an average value of about 23 residues [52], plays an important role in the catalytic cycle [53]. DFG-F at the origin of the segment interacts with the αC-helix and the conserved HRD-H of the catalytic loop. These components are linked hydrophobically as described in Section 3.2 and form part of a regulatory spine. For most protein kinases, the phosphorylation of one–three residues within the activation segment converts an inactive enzyme to a catalytically active enzyme [54,55]. The Raf family contains two phosphorylatable residues within the activation segment (Table 2) ; Zhang and Guan discovered that B-Raf activation requires the phosphorylation of activation segment T598 and S601 [56].

The B-Raf HRD(x)$_4$N-D catalytic-loop aspartate (D576), which is the first D of the K/E/D/D signature, functions as a base and removes a proton from the protein-serine/threonine – OH group thereby enabling the nucleophilic attack of –O: onto the γ-phosphorus atom of ATP (Fig. 5) [57]. The activation segment, when it is in its open conformation, helps to position the protein substrate. β3-K483 forms salt

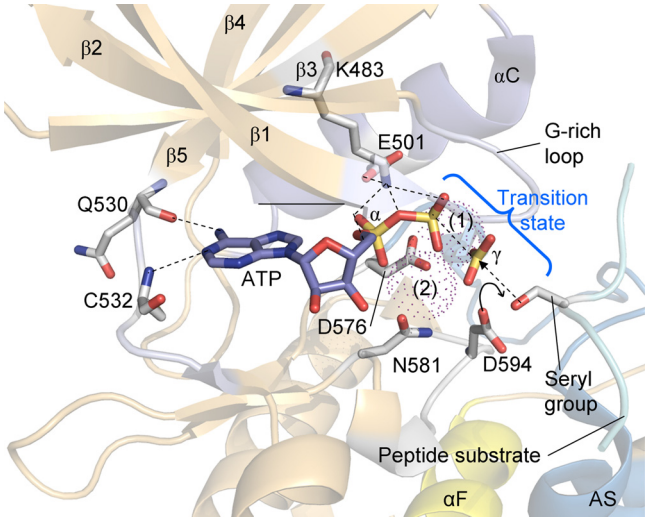

Fig. 5. Inferred mechanism of the B-Raf–catalyzed protein kinase reaction. HRD-D594 abstracts a proton from the protein-serine substrate allowing for its nucleophilic attack onto the γ-phosphorus of ATP. 1 and 2 label the two Mg^{2+} ions shown as dots. AS, activation segment. The figure was prepared from PDB IDs 3QHR 1GY3, but the residues correspond to those of human B-Raf.

bridges with αC-E501 and the α- and β-phosphates of ATP. Extrapolating from PKA [1,49], Mg^{2+}(1) and DFG-D486 bind to the β- and γ-phosphates while Mg^{2+}(2) and β3-K483 bind to the α- and γ-phosphates of ATP thereby aiding catalysis.

The following provides a synopsis of Raf activation. In the absence of upstream signaling activity in normal cells, Raf is hypothesized to adopt a monomeric closed and dormant conformation owing to the intramolecular interaction between the N-terminal regulatory segment and C-terminal protein kinase domain [58]. Following growth factor stimulation and the conversion of Ras-GDP to Ras-GTP in the plasma membrane, Raf is attracted to the membrane concomitant with the formation of a Raf-Ras-GTP complex involving the Ras-binding domain within the amino-terminus of Raf (Fig. 2). Raf kinases become activated following phosphorylation of specific residues such as T599 and S602 in B-Raf and side-to-side homodimerization or heterodimerization involving kinase domain contacts. The dimerization interface includes the αC-helix of each kinase including the C-terminal R509 of B-Raf. The point at which activation segment phosphorylation occurs is unclear. However, following dimerization and activation segment phosphorylation, wild type Raf enzymes become active.

The protein kinase domains of KSR1 and KSR2 have the same overall architecture as the Raf family enzymes (Fig. 2). However, arginine residues substitute for the conserved β3-lysines of classical protein kinases leading to the notion that KSR1/2 are pseudokinases. Brennan et al. have performed experiments indicating that KSR2 possesses protein kinase activity [59]. In contrast to metabolic enzymes such as hexokinase with turnover numbers of hundreds or thousands per second, protein kinases are functional with turnover numbers of a few per minute because the relative concentration of kinase and substrate (which may be present in a one-to-one ratio during autophosphorylation) is similar.

3.2. The hydrophobic spines of the Raf kinase family and KSR1/2

Kornev et al. studied the structures of 23 protein kinases and they determined the role of several essential residues by a local spatial pattern alignment algorithm [60,61]. They characterized and named four hydrophobic residues as a regulatory or R-spine and eight hydrophobic residues as a catalytic or C-spine. Both spines contain amino acid residues from the small and large lobes. The R-spine contains one residue from the activation segment (DFG-F) and another from the regulatory αC-helix, both of which are major components that assume active and inactive conformations. The C-spine positions ATP within the active site cleft to enable catalysis and the R-spine within the carboxyterminal lobe anchors the catalytic loop and activation segment in an active state. Moreover, the precise alignment of both spines is required for the assembly of an active enzyme as described for the ALK receptor protein-tyrosine kinase, the cyclin-dependent protein-serine/threonine kinases, EGFR, ERK1/2, the Janus kinases, Kit, MEK1/2, PDGFRα/β, RET, ROS1, Src, and VEGFR1/2/3 [5,11,14,48,62–72].

Extending from the bottom to the top, the R-spine of protein kinases consists of the catalytic loop HRD-H (RS1), the activation loop DFG-F (RS2), an amino acid four residues C-terminal to the conserved αC-glutamate (RS3), and a hydrophobic amino acid at the beginning of the β4-strand (RS4) [60]. The backbone N—H group of the HRD-H forms a hydrogen bond with an invariant aspartate carboxylate group within the αF-helix (RS0). Again, extending from the bottom to the top of the R-spine, Meharena et al. named the R-spine residues as RS0, RS1, RS2, RS3, and RS4 [73]. The R-spine of active B-Raf with DFG-D_{in} is linear (Fig. 3B). In contrast, the R-spine of dormant B-Raf with DFG-D_{out} is broken with a displaced RS2 residue (Fig. 3D). The R-spine of B-Raf with αC_{out} has RS3 displaced rightward from RS2 and RS4. The distinction between the spine in active B-Raf and αC_{out} B-Raf is subtle (Fig. 3B and D) [74]. The protein kinase C-spine contains amino acid residues from both the N-terminal and C-terminal lobes; moreover, the adenine base of ATP completes the C-spine [61]. The two residues of the N-terminal lobe that interact with the ATP adenine include a conserved alanine from the signature AxK of the β3-strand (CS8) and an invariant valine at the beginning of the β2-strand (CS7). Moreover, a residue from the β7-strand (CS6) on the floor of the adenine pocket interacts hydrophobically with the ATP adenine. Based upon the study of dozens of crystal structures, we find that essentially all steady-state ATP-competitive protein kinase inhibitors interact with CS6. The CS6 residue is found between two hydrophobic residues (CS4 and CS5) that altogether constitute the β7-strand. The CS6 residue interacts with the CS3 residue that occurs near the beginning of the αD-helix of the C-terminal lobe. CS5/6/4 immediately follow the catalytic loop asparagine ($HRD(x)_4N$) so that these residues can be readily identified in the primary structure. The CS3 and CS4 residues interact hydrophobically with CS1 and CS2 within the αF-helix to complete the C-spine (Fig. 3B) [61]. The hydrophobic αF-helix, which spans the entire C-terminal lobe, anchors both the C- and R-spines. Moreover, both spines play a critical role in anchoring the protein kinase catalytic residues in a functional state. CS7 and CS8 in the amino-terminal lobe form part of the "ceiling" of the adenine-binding pocket while CS6 in the carboxyterminal lobe forms part of the "floor" of the binding pocket.

Based upon the findings of site-directed mutagenesis experiments, Meharena et al. identified three shell (Sh) residues in the PKA catalytic subunit that stabilize the R-spine, which they designated as Sh1, Sh2, and Sh3 [73]. The Sh2 residue corresponds to the canonical gatekeeper residue of protein kinases. The gatekeeper residue plays a crucial role in controlling access to the so-called back pocket [75,76] or hydrophobic pocket II (HPII) [76,77]. In contrast to the identification of the APE, DFG, or HRD signatures, which is based upon the primary structure [45], the two spines were identified by their spatial locations in active or dormant protein kinases [60,61]. Table 3 provides a list of the spine and shell residues of the human (i) Raf family, (ii) KSR1/2, (iii) MEK1/2, and (iv) murine PKA. Small molecule protein kinase inhibitors often interact with residues within the C-spine as well as with R-spine and shell residues [78].

4. Interaction of Raf, KSR, and MEK

MEK1 and MEK2 are dual specificity protein kinases that catalyze the phosphorylation of a tyrosine and threonine within the activation segment of ERK1/2 [6,11]. These enzymes contain a short (≈ 70 residues) amino-terminal sequence that occurs before the protein kinase domain. This N-terminal sequence contains an ERK-binding domain (EBD), a nuclear export sequence (NES), and a negative regulatory region (NRR) as depicted in Fig. 2. The protein kinase domain is followed by a carboxyterminal tail that contains 31 amino acid residues. Their key catalytic and structural residues are listed in Table 2 and residues of the regulatory and catalytic spines are listed in Table 3.

Besides the four traditional components in the Ras-Raf-MEK-ERK signaling module, scaffolding proteins such as Kinase Suppressor of Ras (KSR1/2) play an important role in this signaling cascade. KSR functions as a crucial scaffolding protein to coordinate the assembly of Raf-MEK-ERK complexes. Humans possess two KSR genes (*KSR1* and *KSR2*). Their primary structures indicate that KSR1/2 belong to the protein-serine/threonine kinase family. It was first believed that these proteins were catalytically inactive owing to the absence of essential amino acid residues. Although most active protein kinases possess HRD (His-Arg-Asp) or YRD (Tyr-Arg-Asp) at the beginning of the catalytic loop, KSR1/2 have HKD (His-Lys-Asp) in its place in humans (Table 2), *Drosophila* (UniProtKB Q24171), and *C. Elegans* (UniProtKB Q19380). Furthermore, the essential β3-lysine residue within most protein kinases, including the KSR of *Drosophila* and *C. Elegans*, is replaced by an arginine in human KSR1 and KSR2 (R637/R692). Note the presence of these paradoxical mutations; we have the substitution of arginine for lysine within the β-strand and the substitution of lysine for arginine within the catalytic loop. Despite these mutations, KSR1 [79] and KSR2 [59] exhibit some enzyme activity.

Table 3
Spine and shell residues of human (i) A/B/C-Raf, (ii) KSR1/2, (iii) MEK1/2 and (iv) murine PKA.

	Symbol	KLIFS No.	A-Raf	B-Raf	C-Raf	KSR1	KSR2	MEK1	MEK2	PKA[a]
Regulatory spine										
β4-strand (N-lobe)	RS4	38	F369	F516	F408	F772	F725	F129	F133	L106
C-helix (N-lobe)	RS3	28	L358	L505	L397	Y661	Y714	L118	L122	L95
Activation loop F of DFG (C-lobe)	RS2	82	F448	F595	F487	F751	F804	F209	F213	F185
Catalytic loop His/Tyr (C-lobe)	RS1	68	H426	H574	H466	H731	H784	H184	H192	Y164
F-helix (C-lobe)	RS0	None	D491	D638	D530	D803	D856	D245	D249	D220
R-shell										
Two residues upstream from the gatekeeper	Sh3	43	I380	I527	I419	I684	I737	I141	I145	M118
Gatekeeper, end of β5-strand	Sh2	45	T383	T529	T421	T686	T739	M143	M147	M120
αC-β4 loop	Sh1	36	V346	V511	V403	E667	E720	V127	V131	V104
Catalytic spine										
β3-AxK motif (N-lobe)	CS8	15	A334	A481	A373	A637	A690	A95	A99	A70
β2-strand (N-lobe)	CS7	11	V324	V471	V363	V627	V680	V82?	V86	V57
β7-strand (C-lobe)	CS6	77	F436	F583	F475	F740	F793	L197	L201	L173
β7-strand (C-lobe)	CS5	78	L437	L584	L476	Y741	Y794	V198	V202	I174
β7-strand (C-lobe)	CS4	76	I435	I582	I474	V739	V792	I196	I200	L172
D-helix (C-lobe)	CS3	53	L390	L537	L429	L694	L747	L151	L155	M128
F-helix (C-lobe)	CS2	None	L502	L649	L541	L814	L867	S252	S256	L227
F-helix (C-lobe)	CS1	None	V498	V645	V534	V810	I864	M256	L260	M231

[a] From Ref. [60,61].

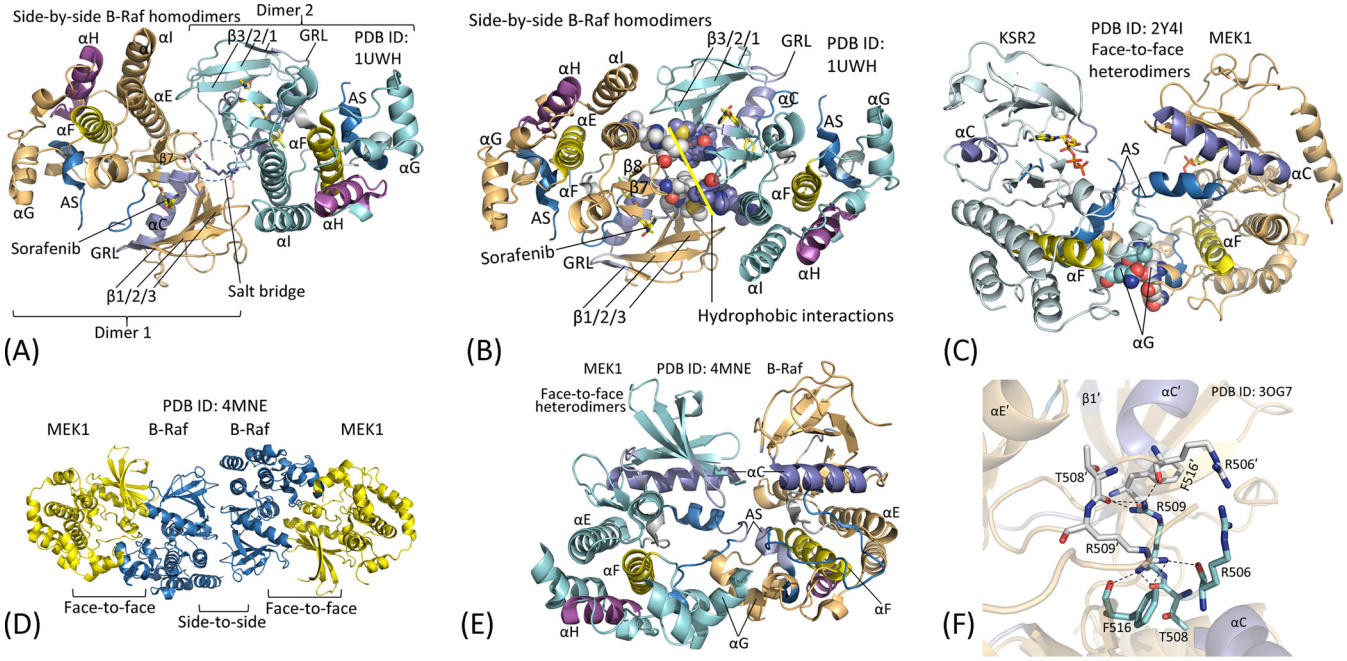

Fig. 6. (A) and (B) B-Raf side-to-side dimers. (C) KSR2–MEK1 face-to-face dimer. (D) MEK1–B-Raf–B-Raf–MEK1 tetramer. (E) B-Raf–MEK1 face-to-face dimers. (F) Salt bridges between the B-Raf side-to-side dimers. The cyan residues belong to the vemurafenib-bound protomer and the gray residues belong to the apo-protomer.

Wan et al. determined the X-ray crystal structure of a B-Raf side-to-side dimer containing sorafenib (Fig. 6 A and B) [80]. The interacting residues in the homodimers involved (i) six residues following the important αC-helix (^{506}RKTRHV^{511}), (ii) three residues in the β3-strand (^{515}LFM^{517}), and (iii) four residues within the αE-helix: D565, Y566, A569, and K570. Hydrogen bonds form from one monomer's R506, T508, F516 with residue R509 of the partner (Fig. 6F). Moreover, H510 and V511 from the αC-β4 back loop of one dimer interact hydrophobically with L515 and M517 from the back loop of the partner dimer. These residues are conserved within the Raf family kinases and KSR1/2. It is hypothesized that the formation of side-to-side dimers is required for the activation of wild type Raf family protein kinases [5]. However, it is unclear whether this occurs before or after phosphorylation of the activation segment (T599 and S602 in B-Raf). There are three possible combinations of Raf homodimers (A-A, B-B, C-C) and three possible combinations of Raf heterodimers (A-B, A-C, B-C). B–C and C–C appear to be the most important signaling dimers.

McKay et al. studied the interaction of KSR1 with B-Raf and MEK [81]. Based upon site-directed mutagenesis and co-immunoprecipitation studies, they identified MEK1 M308 and I310 as residues important for binding with KSR1. Based upon the X-ray crystal structure of the KSR2–MEK1 complex (PDB ID: 2Y4I), these two MEK1 residues make hydrophobic contact with KSR2 L822, Q839, and I883. They also discovered that MEK1 M308/I310 contribute to its interaction with B-Raf. In cells, the KSR1–MEK1 interaction is constitutive under basal conditions and serves to sequester MEK1 from participating in signaling. In signaling cells, however, KSR1 facilitates B-Raf interaction with MEK through the formation of a MEK–KSR1–B-Raf ternary complex. KSR1 of the ternary complex binds to ERK. ERK has the potential to catalyze the phosphorylation of inhibitory feedback sites within B-Raf and KSR2.

Rajakulendran et al. hypothesized that KSR activates B-Raf following the formation of side-to-side heterodimers [82]. Based upon analytical ultracentrifugation, they reported that KSR and Raf form heterodimers, which was abolished by the KSR2 R732H mutation at the dimer interface. Using *Drosophila* S2 cells, they discovered that increasing the content of KSR resulted in MEK phosphorylation that was Ras-independent. Mutation of four other residues in the hypothesized KSR dimerization domain (G700 W, F739 A, M740 W, and Y790 F) also abolished MEK phosphorylation as a result of the failure to activate B-Raf. They hypothesized that KSR has two distinct functions; it first activates Raf following their heterodimerization and it also recruits MEK to facilitate downstream signaling.

Brennan et al. performed structural and biochemical experiments to determine the mechanism of KSR2-stimulated MEK1 phosphorylation as catalyzed by B-Raf [59]. Based upon gel filtration studies, they demonstrated that KSR2–MEK1 exist as tetramers and dimers in solution. MEK1–KSR2 heterodimers assemble into tetramers through a KSR2 side-to-side homodimer interface centered on Arg718. The equilibrium between the dimers and tetramers indicates a weak KSR2 side-to-side homodimer interaction. They determined the crystal structure of the rabbit KSR2-human MEK1 complex and discovered that their active sites face each other and the heterodimer interface includes their activation segments and αG-helices. MEK1–KSR2 form face-to-face heterodimers that involve a hydrogen bond between the carbonyl group of KSR2 K821 and the N−H group of G225 as well as hydrophobic interactions with residues from each member's αG-helix involving KSR2 A881 and Q885 with MEK1 L235 and Q236 (Fig. 6C). These investigators reported that the KSR2 scaffold assembles a MEK1–KSR2–B-Raf ternary complex that is responsible for promoting MEK1 phosphorylation by B-Raf. Brennan et al. discovered that a KSR2 Arg718His mutation abolishes the activation of MEK1 by B-Raf thereby demonstrating the importance of the KSR2 dimer interface in the overall process of MEK1 activation [59].

Brennan et al. found that adding a kinase-dead B-Raf (β3-K483S) mutant to KSR2-MEK1 increases MEK1 phosphorylation 15-fold [59]. A KSR2 inhibitor (ASC24) blocks 70% of total MEK1 phosphorylation, but less than 10% of MEK1 S218/S222 activation segment phosphorylation. Sorafenib, a Raf multikinase inhibitor, blocks 30% of total MEK1 phosphorylation, but more than 90% of MEK1 S218/S222-specific phosphorylation. They inferred that KSR2 is the major enzyme responsible for MEK1 phosphorylation and this results from a B-Raf (β3-K483S)-induced increase in KSR2 enzymatic activity. KSR2-mediated phosphorylation of MEK1 outside of the activation segment may enable B-Raf–mediated phosphorylation of the MEK1 activation segment S218 and S222. These experiments demonstrate that KSR2 possesses catalytic activity despite lacking the canonical residues in the β3-strand and catalytic loop as noted above. B-Raf forms active side-to-side homodimers [58] and B-Raf apparently stimulates KSR2 activity allosterically by forming similar heterodimers. KSR2 promotes the release of the MEK1 activation segment for phosphorylation. Brennan et al. hypothesize that regulatory B-Raf interacts with KSR2 in *cis* to introduce a conformational change in KSR2 thereby facilitating phosphorylation of MEK1 by an independent catalytic B-Raf molecule in *trans* (Fig. 7A).

Lavoie et al. studied the interaction of B-Raf, MEK1/2, and KSR1 [43]. They discovered that MEK1 or MEK2 induces B-Raf–KSR1 kinase domain side-to-side dimerization and this process was independent of MEK catalytic activity. The ability of MEK1 to promote B-Raf–KSR1 complex formation was dependent on KSR–MEK interaction and was abolished by mutations involving αG-helix dimerization residues. B-Raf–KSR1 complex formation was also dependent on the ability of these two proteins to form side-to-side dimers. These investigators hypothesized the existence of two functionally unique MEK proteins, i.e., an activator MEK that binds to KSR1 and stimulates dimerization with B-Raf and a substrate MEK that interacts with and is phosphorylated in a reaction catalyzed by B-Raf. This scheme is illustrated in Fig. 7B.

Both schemes begin with a KSR side-to-side homodimer with each protomer bound face-to-face with MEK (Fig. 7A and B). In scheme I, a regulatory Raf displaces a KSR-MEK heterodimer and binds to MEK–KSR to form a ternary complex; the KSR2–Raf interact in a side-to-side fashion while MEK1–KSR2 interact in a face-to-face manner. An active catalytic Raf homodimer catalyzes the phosphorylation of MEK within the ternary complex. The initial state in scheme II resembles that of scheme I. Now B-Raf displaces a MEK–KSR face-to-face heterodimer to form a ternary complex; in this ternary complex, B-Raf is activated by its side-to-side interaction with KSR. The activated B-Raf then catalyzes the phosphorylation of substrate MEK. It is unclear at which step B-Raf activation segment phosphorylation occurs during the activation process. Whether scheme I, scheme II, a combination of them, or other schemes for MEK activation are employed by nature will require additional experimentation. Thus, future work will be required to firmly establish the mechanism that leads to MEK activation in a process involving Raf, MEK, and KSR.

Haling et al. determined the X-ray crystal structure of the B-Raf–MEK1 complex and found a tetramer that consisted of a dimer of the B-Raf–MEK1 complex (Fig. 6D) [83]. Two central B-Raf protomers form a side-to-side transactivating dimer while the MEK1–B-Raf portion consists of a face-to-face dimer with MEK1 that involves the interaction of the respective activation segments (Fig. 6E). The B-Raf G615 carbonyl group hydrogen bonds with the N−H group of MEK1 V225 and the N−H group of B-Raf I617 hydrogen bonds with the carbonyl group of MEK1 S222 (not shown). These investigators discovered that the B-Raf I617R mutation completely disrupts its binding to MEK1. The activation of MEK1 requires the phosphorylation of S218 and S222 within the activation segment [6]. The face-to-face interactions also involve interactions between the αEF and αG-helices. The activation segment of B-Raf is in an active (but unphosphorylated) and open conformation while that of MEK1 is in an inactive closed conformation. The face-to-face interactions resemble those formed between KSR2 and MEK1. However, B-Raf and MEK1 exist in solution as a stable tetramer (MEK1–B-Raf–B-Raf–MEK1) while KSR2 and MEK1 exist as a dimer (MEK1–KSR2) and tetramer (MEK1–KSR2–KSR2–MEK1) in equilibrium.

5. FDA-approved B-Raf and MEK1/2 inhibitors

5.1. Classification of protein kinase-drug complexes

Dar and Shokat defined three classes of small molecule protein kinase antagonists and labeled them types I, II, and III [84]. The type I inhibitors bind within the ATP pocket of an active protein kinase; the type II inhibitors bind to an inactive protein kinase with the activation segment DFG-D pointing away from the active site (DFG-D_{out}) while the type III inhibitors bind to an allosteric site, which is not part of the active site [85] and is external to the ATP-binding site. Zuccotto subsequently defined type I½ inhibitors as drugs that bind to an inactive protein kinase with the DFG-D pointed inward (DFG-D_{in}) toward the active site (in contrast to the DFG-D_{out} conformation) [86]. The dormant enzyme may display an αC-$helix_{out}$ conformation, a closed activation segment, or a nonlinear or broken regulatory spine. Gavrin and Saiah subsequently divided allosteric inhibitors into two types: III and IV [87]. The type III inhibitors bind within the cleft between the small and large lobes and next to, but independent of, the ATP binding site while type IV allosteric inhibitors bind elsewhere. Moreover, Lamba and Gosh defined bivalent antagonists as those inhibitors that span two distinct parts of the protein kinase domain as type V inhibitors [88]. For example, an inhibitor that bound to the ATP-binding site as well as the peptide substrate site would be classified as a type V inhibitor. To complete this classification, we named inhibitors that bind covalently with the target enzyme as type VI antagonists [78]. For example, afatinib is a type VI covalent inhibitor of EGFR that is FDA-approved for the treatment of NSCLC. Mechanistically, this drug binds initially and reversibly to an active EGFR conformation (like a type I inhibitor) and

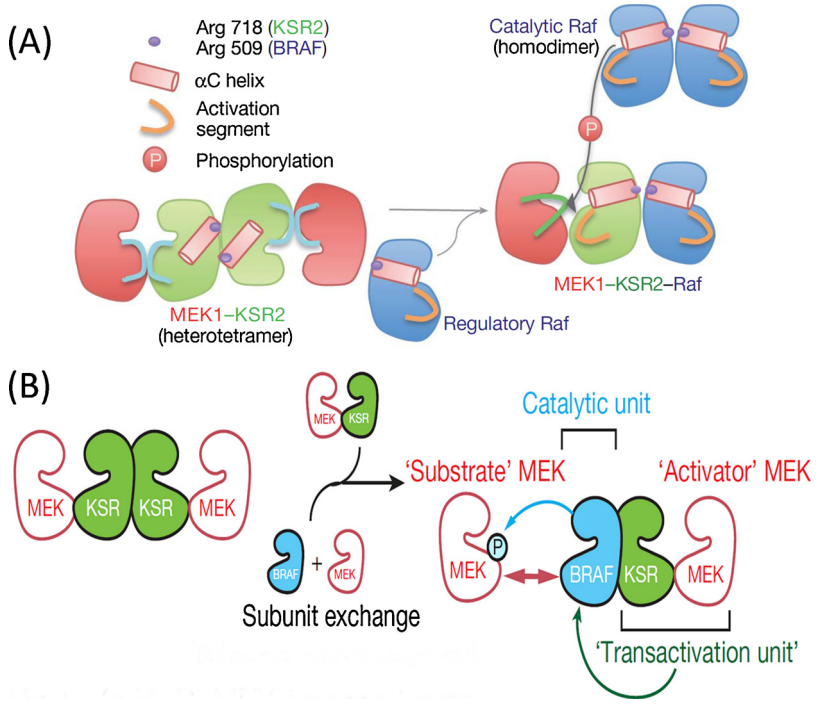

Fig. 7. (A) Regulatory and catalytic Raf. Reproduced from Ref. [59] with copyright permission of Springer Nature. (B) Activator and substrate MEK1. Reproduced from Ref [43]. with copyright permission of Springer Nature.

then the thiol group of EGFR C797 attacks the drug to form an irreversible covalent adduct [78].

Owing to the diversity of inactive conformations when compared with the conserved active protein kinase conformation, it was hypothesized that type II inhibitors would be more selective than type I inhibitors, which bind to the canonical active conformation. The assessment of Vijayan et al. corroborate this hypothesis [51] while those of Kwarcinski et al. and Zhao et al. do not [89,90]. Type III allosteric inhibitors bind next to the adenine binding pocket [87]. Owing to the greater variance in this region when compared with the ATP binding pocket, type III antagonists have the potential to be more selective than type I, I½, or II inhibitors. The studies of Kwarcinski et al. suggest that antagonists that bind to the αC_{out} conformation (type I½ inhibitors) may be more selective than type I and II inhibitors [89]. FDA-approved αC_{out} inhibitors include neratinib – an ErbB2/HER2 antagonist – and lapatinib – an EGFR/ErbB1 and ErbB2/HER2 antagonist – both drugs of which are used in the treatment of advanced breast cancer. However, their studies suggest that not all protein kinases are able to assume the αC_{out} conformation while they indicate that all kinases are able to adopt the DFG-D_{out} conformation.

We previously divided the type I½ and type II inhibitors into A and B subtypes [78]. As described in Section 6, sorafenib is a type II inhibitor of B-Raf (PDB ID: 1UWH). This drug binds to the DFG-D_{out} configuration of the protein kinase domain and extends into the back cleft. We classified drugs that extend into the back cleft as type IIA inhibitors. In contrast, we classified drugs that (i) bind to the DFG-D_{out} conformation and (ii) do not extend into the back cleft as type IIB inhibitors. Based upon limited data, the possible significance of this distinction is that type A inhibitors bind to their target enzyme with a longer residence time when compared with type B inhibitors [78].

Type II inhibitors bind to their target protein kinase with the DFG-D directed away from the active site [2,78,91] and they are usually the easiest to identify by inspection. As a consequence, the DFG-D and DFG-F switch places and the change in location of the phenylalanine residue creates a large allosteric site that interacts with a portion of type II antagonists such as sorafenib. The adenine-binding site occurs within the front pocket and does not project past the gate area into the back pocket. In Section 6, we will see that the B-Raf antagonists studied in this paper are type I½ and type IIA inhibitors.

Ung et al. examined a range of structural features based upon the disposition of the αC-helix and the DFG motif to define the conformation space of the catalytic domain of protein kinases [74]. They note that the αC-helix can move from its active αC_{in} position to the αC_{out} position by tilting and rotation. Similarly, the DFG motif can move from its active DFG-D_{in} position to the inactive DFG-D_{out} position. These investigators defined five different protein kinase conformations: αC_{in}-DFG-D_{in} (CIDI), αC_{in}-DGF-D_{out} (CIDO), αC_{out}-DFG-D_{in} (CODI), αC_{out}-DFG-D_{out} (CODO), and ωCD representing structures with variable DFG-D intermediate states or variable positions of the αC-helix. CIDI represents the catalytically active state with an intact R-spine. Type I protein kinase inhibitors compete with ATP for its binding pocket and interact with the hinge region. CIDO has the DFG motif flip that reshapes the ATP-binding site and displaces DFG-F thereby breaking the R-spine (Fig. 3D). Many type II protein kinase inhibitors occupy the DFG-pocket and form hydrogen bonds with the DFG-D backbone amide and the αC-E carboxylate. CODI denotes the αC_{out} and DFG-D_{in} conformation and has an intact R-spine. The folding of the activation loop deforms the protein-substrate binding site while also displacing the αC-helix to its dilated or to its out configuration. The movement of the αC-helix allows for the binding of vemurafenib to B-Raf as described in Section 6. CODO has both αC_{out} and DFG-D_{out} with a distorted R-spine. There are only limited structural data on the CODO conformations and few known bound ligands. ωCD structures are highly heterogeneous with diverse DFG-D intermediate states and variable αC-helix positioning. ωCD configurations may represent transition states among the various primary conformations.

5.2. Drug-ligand binding pockets

Liao [77] and van Linden et al. [92] divided the region between the protein kinase amino-terminal and carboxyterminal lobes where ATP binds into a front cleft or pocket, a gate area, and a back cleft. The back pocket or HPII (hydrophobic pocket II) includes the gate area and back cleft (Fig. 8). The front cleft includes the adenine pocket, the hinge

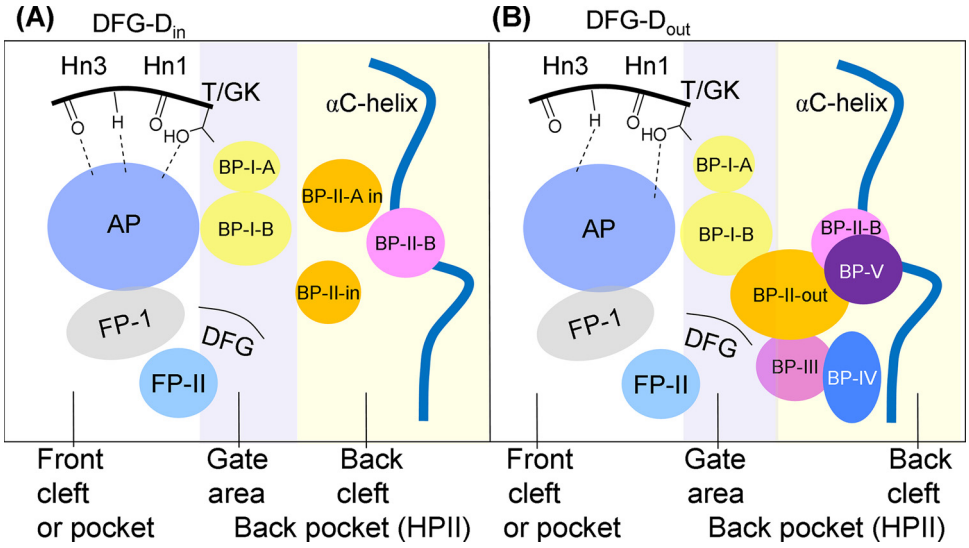

Fig. 8. Location of the protein kinase domain drug-binding pockets. AP, adenine pocket; BP, back pocket; FP, front pocket; Hn, hinge; HPII, hydrophobic pocket II; T/GK, threonine/gatekeeper. Adapted from Refs. [77,92].

residues, the glycine-rich loop, the extension connecting the hinge residues to the large lobe αD-helix, and the amino acid residues within the catalytic loop (HRD(x)$_4$N). The gate area includes the β3-strand of the small lobe and the proximal portion of the activation segment including DFG. The back cleft extends to the αC-helix, the αC-β4 back loop, portions of the β4- and β5-strands of the amino-terminal lobe and a section of the αE-helix within the carboxyterminal lobe.

van Linden et al. identified several sub-pockets that are found in these three regions [92]. For example, the front cleft includes an adenine-binding pocket (AP) adjacent to two front pockets (FP-I and FP-II). FP-I occurs between the solvent-exposed extension that connects the hinge residues to the αD-helix and the xDFG-motif (where x is the residue immediately before the activation segment DFG) and FP-II is found between the glycine-rich loop and the β3-strand at the top of the cleft. Back pocket I (BP-I), which can be divided into two subpockets (BP-I-A and BP-I-B), is located in the gate area between the xDFG-motif, the β3- and β4-strands, the conserved β3-K of the AxK signature, and the αC-helix. The smaller BP-I-A occurs at the top of the gate area and is bordered by residues of the β3- and β5-strands including the β3-AxK and the αC-helix. The larger BP-I-B is found at the center of the gate area permitting access to the back cleft. BP-I-A and BP-I-B occur in the DFG-D$_{in}$ and DFG-D$_{out}$ conformations (Fig. 8).

BP-II-A-in and BP-II-in occur within the back cleft in the DFG-D$_{in}$ conformation [77]. These pockets are bordered by the large lobe DFG-motif and the small lobe αC-helix, the αC-β4 back loop, and the β4- and β5-strands. Major modification of BP-II-A-in and BP-II-in takes place to produce BP-II-out in the DFG-D$_{out}$ configuration; this conversion occurs with a change in the location of DFG-F. The resulting compartment is named back pocket II-out (BP-II-out); it is found where the DFG-F occurs in the DFG-D$_{in}$ configuration. BP-II-B is bordered by the αC-helix and β4-strand in both the DFG-D$_{in}$ and DFG-D$_{out}$ conformations. Back pocket III (BP-III) is found only in the DFG-D$_{out}$ conformation. This compartment occurs on the floor of BP-II-out between the activation segment DFG-D$_{out}$ motif, the conserved catalytic loop HRD-H, the β6-strand, and the αE-helices of the large lobe and the αC-β4 back loop and the αC-helices of the small lobe. Two pockets that are partially solvent exposed (BP-IV and BP-V) occur between the small lobe αC-helix and the large lobe DFG-D$_{out}$ motif, the catalytic loop, the β6-strand, and the activation segment (Fig. 8).

van Linden et al. formulated a comprehensive summary of drug and ligand binding to more than 1200 human and mouse protein kinase domains [92]. Their KLIFS (kinase–ligand interaction fingerprint and structure) directory includes an alignment of 85 ligand binding-site residues occurring in both the amino-terminal and carboxyterminal lobes; this catalog expedites the classification of drugs and ligands based upon their binding characteristics and facilitates the detection of related interactions. Moreover, these investigators devised a standard amino acid residue numbering system that facilitates the comparison of many protein kinases. Table 3 specifies the relationship between the KLIFS database numbering and the catalytic spine, shell, and regulatory spine amino acid residue nomenclature. Moreover, this group established a valuable free and searchable web site that is regularly updated thereby providing comprehensive information on protein kinase interaction with drugs and ligands (klifs.vu-compmedchem.nl/).

6. Structures of Raf-drug complexes

Vemurafenib (Fig. 9A) is a 7-azaindole derivative that is FDA-approved for the treatment of *BRAF*$^{V600E/K}$ mutant (i) advanced melanoma or (ii) Erdheim-Chester disease (Table 4). The latter malady is a rare illness characterized by the abnormal proliferation of histiocytes (a tissue macrophage or a dendritic cell); about half of the people with this illness possess the *BRAF*^{V600E} mutation. The name vemurafenib is derived from V600E mutant B-Raf inhibition. The drug is a multikinase inhibitor with activity against B-Raf^{V600E}, SRMS, ACK1, MAP4K5, and FGR (www.brimr.org/PKI/PKIs.htm). Bollag et al. provided a comprehensive summary that led to the development of vemurafenib [93]. These investigators screened small molecules (150–350 Da) with fewer than eight hydrogen bond donors and acceptors with few rotatable bonds against five different protein kinases to identify potential scaffolds. Some 238 compounds were selected for co-crystal structure analysis and more than 100 structures of protein kinases with PIM1 and FGFR1 were determined while the methodology for preparing B-Raf crystals was being developed. A 3-substituted 7-azaindole was chosen for further optimization based upon its binding to PIM1. After finding the most favorable compounds based upon binding affinity, selectivity, and pharmacokinetic properties as well as solving the X-ray crystal structures of more than 100 compounds bound to B-Raf, vemurafenib was the final product.

The X-ray structure of vemurafenib bound to B-Raf^{V600E} (PDB ID: 3OG7) shows that the *N*1 nitrogen of the azaindole group forms a hydrogen bond with the carbonyl group of Q530 (the first hinge residue), the *N*7 N−H group of the drug makes a hydrogen bond with C532 (the third hinge residue), and the sulfonamide oxygen forms hydrogen bonds with the N−H groups of DFG-F595 and DFG-G596 (Fig. 10A). The drug makes hydrophobic contact with I463 at the end of the β1-

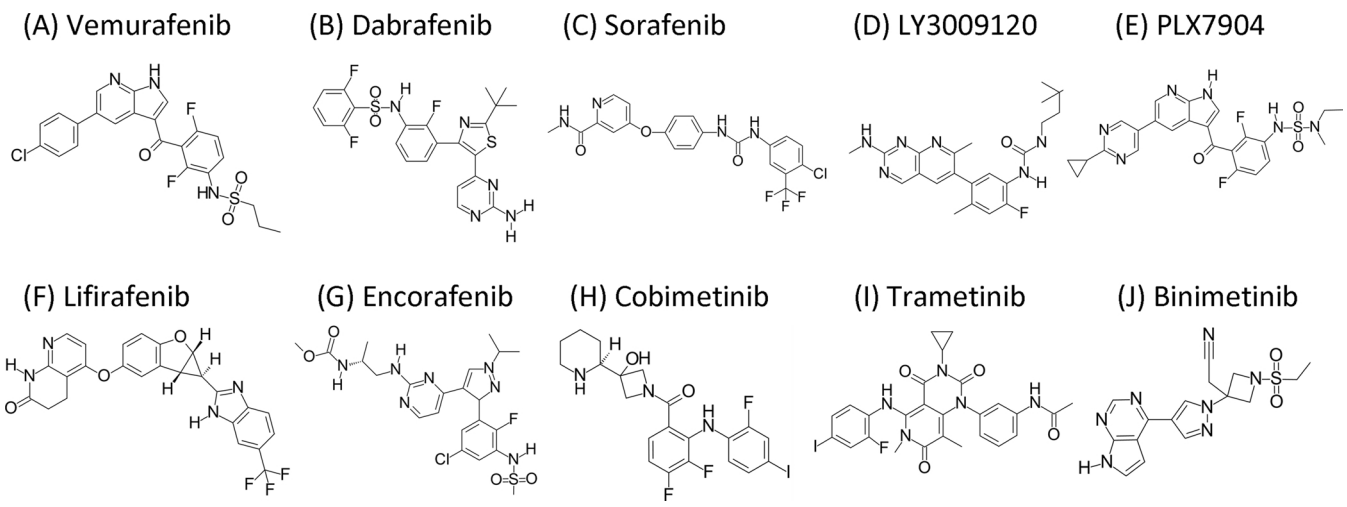

Fig. 9. Structures of selected Raf (A–G) and MEK inhibitors (H–J).

strand, V471 in the β2-strand after the G-rich loop, β3-strand A481 and K483, L505 in the αC-helix (RS3), L514 in the αC-β4 back loop, I527 near the end of the β5-strand, W531 within the hinge, and F583 within the β7-strand (CS6). The drug makes van der Waals contact with DFG-D594. Vemurafenib binds within the front pocket (FP-I), gate area (BP-I-A, BP-I-B), and back cleft (BP-II-A-in, BP-II-in). The drug binds to an inactive conformation (αC_{out}) with DFG-D_{in} and is therefore classified as a type I½ inhibitor [78].

Dabrafenib (Fig. 9B) is an aminopyrimidine thiazole derivative that is FDA-approved as a single agent for the treatment of unresectable or metastatic melanoma with *BRAF*$^{V600E/K}$ mutations or as part of a combination of drugs (with trametinib) for the treatment of metastatic melanoma or NSCLC with *BRAF*$^{V600E/K}$ mutations (Table 4). Rheault et al. described the development of this medicinal from a lead thiazole compound that involved modification of a headgroup and tail to improve its pharmacokinetic properties while preserving favorable target selectivity and potency [94]. The X-ray structure of dabrafenib bound to B-Raf^{V600E} (PDB ID: 4XV2) shows that the *N1* of the pyrimidine forms a hydrogen bond with the N—H group of C532 of the hinge and the 2-amino group attached to the pyrimidine forms a hydrogen bond with the C532 carbonyl group while one of the sulfonamide oxygens forms a hydrogen bond with the β3-strand K483 and the other sulfonamide oxygen forms a hydrogen bond with the N—H group of DFG-F595 (Fig. 10B). The drug makes hydrophobic contact with I463 at the end of the β1-strand, F468 within the G-rich loop, V471 within the β2-strand, the β3-strand A481 (CS8) and K483, L505 within the αC-helix (RS3), L514, L515, and F516 in the αC-β4 loop, I527 within the β5-strand, Q530 and W531 within the hinge, F583 within the β8-strand (CS6). The drug also makes van der Waals contact with DFG-D594. Dabrafenib binds within the front pocket (FP-I), gate area (BP-I-B), and the back pocket (BP-II-A-in, BP-II-in). The drug binds to an inactive conformation (αC_{out}) with DFG-D_{in} and is therefore classified as a type I½ inhibitor.

Sorafenib (Fig. 9C) is a pyridine carboxamide bis aryl-urea derivative that is FDA-approved for the treatment of hepatocellular carcinomas, renal cell carcinomas, and differentiated thyroid carcinomas that are refractory to radioiodine treatment. The agent is a multikinase inhibitor with activity against B/C-Raf, B-Raf^{V600E}, Flt3, Kit, RET, VEGFR1/2/3, and PDGFRβ (Table 4) [95,96]. It was initially developed as a Raf inhibitor as indicated by its name (sorafenib). Its effects against renal cell carcinomas is most likely related to its inhibition of the VEGFR family of receptor protein-tyrosine kinases. The X-ray crystal structure of sorafenib bound to B-Raf shows that the pyridine *N1* forms a hydrogen bond with the N—H group of C532 and the carboxamide N—H forms a hydrogen bond with the carbonyl group of C532 within the hinge. The αC-E501 forms a hydrogen bond with each of the urea

Table 4
Selected properties of orally effective Raf multikinase and MEK inhibitors.

Name, code, trade name	Selected targets	Type[a]	Formula	MW (Da)	D/A[b]	RB[c]	FDA-approved indications (year of initial approval)[d]
Vemurafenib, PLX4032, Zelboraf	A/B/C-Raf, B-Raf V600E, SRMS, ACK1, MAP4K5, FGFR	I½	$C_{22}H_{24}BrFN_4O_2$	489.9	2/7	7	Melanoma with *BRAF*^{V600E}mutation and Erdheim-Chester disease (2011)
Dabrafenib, GSK2118436, Tafinlar	B-Raf	I½	$C_{23}H_{20}F_3N_5O_2S_2$	519.6	2/11	6	Melanoma (2013) and NSCLC (2017) with *BRAF* mutations
Sorafenib, BAY 43-9006, Nexavar	B/C-Raf, B-Raf V600E, Kit, Flt3, RET, PDGFRβ, VEGFR1/2/3,	IIA	$C_{21}H_{16}ClF_3N_4O_3$	464.8	3/7	5	Hepatocellular carcinoma, RCC, DTC (2005)
LY3009120	A/B/C-Raf	IIA	$C_{23}H_{29}FN_6O$	424.5	3/6	6	Clinical trial NCT02014116 for melanoma and other advanced cancers
PLX7904	B-Raf	I½	$C_{24}H_{22}F_2N_6O_3S$	512.5	2/10	8	No current clinical trials
Lifirafenib	B-Raf	IIA	$C_{25}H_{17}F_3N_4O_3$	478.4	2/8	3	Clinical trial NCT02610361 for solid tumors
Encorafenib	B-Raf	?	$C_{22}H_{27}ClFN_7O_4S$	540.0	3/10	10	Melanoma B-Raf$^{V600E/K}$ with binimetinib (2018)
Cobimetinib, GDC-0973	MEK1/2	III	$C_{21}H_{21}FIN_3O_2$	531	4/7	4	Melanoma B-Raf$^{V600E/K}$ with vemurafenib
Trametinib, GSK1120212	MEK1/2	III	$C_{32}H_{23}FIN_5O_4$	615.0	2/6	5	Melanoma (2013) & NSCLC (2017) with *BRAF* mutations
Binimetinib, MEK-162	MEK1/2	?	$C_{17}H_{15}BrF_2N_4O_3$	441.2	3/7	6	Melanoma B-Raf$^{V600E/K}$ with encorafenib (2018)

[a]Type of inhibitor based upon the drug-kinase structure as described in Ref. [78].
[b]D, no. of hydrogen bond donors; A, no. of hydrogen bond acceptors.
[c]No. of rotatable bonds.
[d]DTC, differentiated thyroid cancer; NSCLC, non-small cell lung cancer; RCC, renal cell carcinoma.

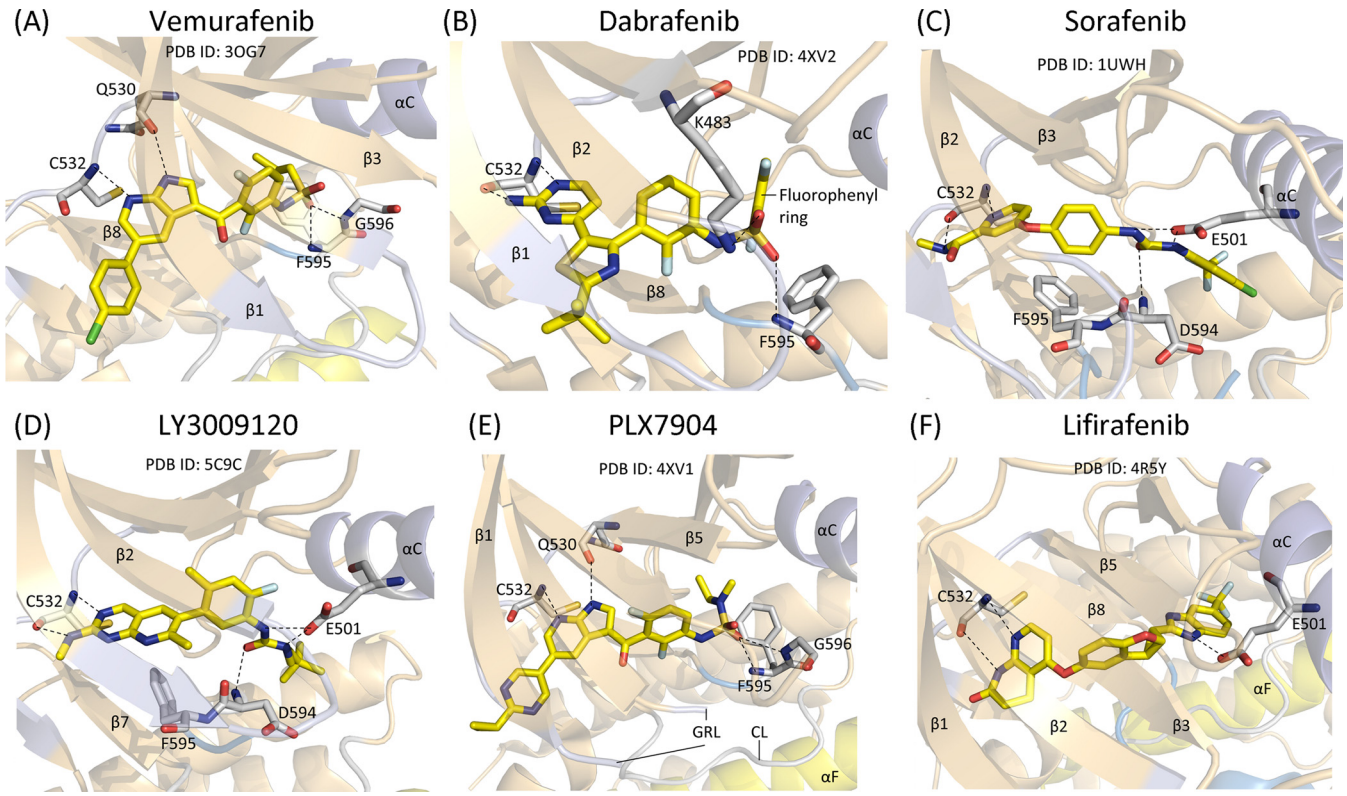

Fig. 10. Structures of B-Raf–drug complexes. The carbon atoms of the drugs are colored yellow. CL, catalytic loop; GRL, glycine-rich loop. The dashed lines depict polar bonds.

N—H groups and the urea oxygen forms a polar bond with the N—H group of DFG-D594. The drug makes hydrophobic interactions with I463 at the end of the β1-strand, V471 within the β2-strand, A481 (CS8) and K483 in the β3-strand, V504 and L505 (RS3) within the αC-helix, Q530 and W531 within the hinge, L567 and I572 before the catalytic loop, HRD-H574 of the catalytic loop, F583 (CS6), and DFG-F595. Sorafenib binds within the front pocket, gate area, and back pocket (BP-I-B, BP-II-out, and BP-III). Because it binds to the DFG-D_{out} configuration and extends into the back pocket, it is classified as a type IIA inhibitor.

LY3009120 (Fig. 9D) is a pyridopyrimidine phenyl urea derivative that is in clinical trials for melanoma and other advanced cancers (Table 4). This agent has demonstrated antitumor activity in xenograft studies with *KRAS* or *NRAS* mutant neoplasms as well as vemurafenib-resistant melanomas [97,98]. It is also effective against B-Raf β3-αC deletions that have been found in pancreatic and thyroid tumors [99]. LY3009120 inhibits monomeric and dimeric B-Raf with similar potency. The X-ray crystal structure of LY3009120 bound to B-Raf shows that *N*1 of the pyridopyrimidine moiety forms a hydrogen bond with the N—H group of C532 and the methylamino N—H group forms a hydrogen bond with the carbonyl group of C532, the third hinge residue. Each of the two urea N—H groups makes polar contact with E501 while the urea oxygen forms a polar bond with DFG-D594. The drug makes hydrophobic contact with V471 of the β2-strand, A481 (CS8) and K483 within the β3-strand, L505 (RS3) within the αC-helix, L513 in the αC-β4 back loop, I527 within the β5-strand, Q530 and W531 within the hinge, L567 before the catalytic loop, HRD-H574 (RS1), I592 before the activation segment, and DFG-F595 (RS2). LY3009120 binds within the front pocket, gate area, and back pocket (BP—I—B and BP-III). Note that its binding to B-Raf closely resembles that of sorafenib (Fig. 10C and D). Because it binds to the DFG-D_{out} configuration and extends into the back pocket, it is classified as a type IIA inhibitor [78].

PLX7904 (Fig. 9E) is a 7-azaindole derivative that is a next generation B-Raf inhibitor that is in its early stages of development; this agent has greater potency against B-Raf ^{V600E} than vemurafenib [100]. It is considered to be a paradox breaker because it suppresses mutant B-Raf without activating the MAP kinase pathway in cells that possess *RAS* mutations or elevation of receptor protein-tyrosine kinase activity. The X-ray crystal structure shows that the *N7* N—H group of the azaindole forms a hydrogen bond with the carbonyl group of the first hinge residue (Q530) and the *N1* of the azaindole forms a hydrogen bond with the N—H group of the third hinge residue (C532). One of the sulfamide oxygens forms hydrogen bonds with the N—H groups of both DFG-F595 and DFG-G596 (Fig. 10E). The drug makes hydrophobic contact with I463 at the end of the β1-strand, V471 near the beginning of the β2-strand, β3 A481 (CS8) and K483, αC-L505 (RS3), L514 and F516 in the αC-β4 loop, I527 of the β5-strand, W531 (the second hinge residue), F583 (CS6), and DFG-F595. The drug also makes van der Waals contact with DFG-D594. The drug binds within the front pocket (FP-I), gate area (BP-I-A, BP-I-B), and back pocket (BP-II-A-in, BP-II-in). Note that the binding of PLX7904 to B-Raf closely resembles the binding of vemurafenib (PLX4032) to the enzyme (Fig. 10A and E). PLX7904 is a type I½ inhibitor that binds to a αC_{out}–DFG-D_{in} (CODI) inactive conformation.

Lifirafenib (Fig. 9F) is a fused tricyclic benzimidazole (Fig. 9F) that inhibits both B-Raf and EGFR and is in its early stages of development [101]. The IC_{50} values of the drug for B-Raf^{V600E} (23 nM), wild type B-Raf (32 nM), C-Raf (7 nM), A-Raf (5.6 nM), and EGFR (29 nM) are in the low nM range. These data demonstrate that lifirafenib is a pan-Raf inhibitor, which suggests that it will not give rise to the paradoxical activation of the MAP kinase pathway. Tang et al. reported that lifirafenib was effective in the treatment of the human *BRAF^{V600E}* WiDr colorectal xenograft model [101]. Owing to the presence of B-Raf^{V600E}-mutations along with increased activity of EGFR in some forms of colorectal cancer, this single agent has the potential to block each of these oncogenic activities. The X-ray crystal structure shows that the nitrogen atom on the pyridine lactam groups forms a hydrogen bond with the carbonyl group of C532 while the *N1* of the pyridine forms a hydrogen

bond with the N—H of C532 (Fig. 10F). Moreover, the nitrogen atom from the benzimidazole forms a hydrogen bond with the carboxyl group of the αC-E501. The drug makes hydrophobic contact with the β1-strand I463 before the G-rich loop, V471 near the proximal portion of the β2-strand, the β3 A481 (CS8) and K483, L505 (RS3) within the αC-helix, I513 and L514 in the back loop, I527 within the β5-strand, Q530 and W531 within the hinge, L567 before the catalytic loop, HRD-H574 (RS1), F583 (CS6), and DFG-F595 (RS2). Lifirafenib also makes van der Waals contact with DFG-D582. The agent binds to the front pocket, the gate area (BP-I-A and BP-I-B), and back pocket (BP-III). The drug binds to the DFG-D_{out} conformation of B-Raf and extends into the back pocket thereby making it a type IIA inhibitor.

Encorafenib (Fig. 9G) is an imidazole pyridine derivative that is FDA-approved for the treatment of $BRAF^{V600E/K}$-mutant melanoma in combination with binimetinib. Its cellular profiles resemble the αC_{out} B-Raf inhibitors, but its X-ray crystal structure has not been reported to confirm this notion. Encorafenib, binimetinib, and cetuximab combination therapy is being clinically tested in the treatment of $BRAF^{V600E}$-mutant metastatic colon cancer. Cetuximab is a chimeric human/mouse monoclonal antibody directed against EGFR that is FDA-approved for the treatment of wild type *KRAS* mutant colon cancer. The rationale for this study is that the combined inhibition of EGFR and the Ras-Raf-MEK-ERK pathway will be more efficacious in the treatment of these cancers than inhibition of either EGFR or the MAP kinase pathway. Table 4 lists the three MEK inhibitors that have been FDA-approved for the treatment of *BRAF* mutant melanomas and their structures are given in Fig. 9. The current standard of care for *BRAF* mutant melanoma is to use a combination of B-Raf and MEK inhibitors. The superiority of one combination compared with others has not been determined.

7. Classes of *BRAF* mutants

In addition to the $BRAF^{V600E}$ mutation, approximately 200 other B-Raf mutant alleles have been discovered in human neoplasms [102]. Yao et al. divided oncogenic *BRAF* mutants into three classes that determine their sensitivity to targeted inhibitors [103]. Class 1 mutants ($BRAF^{V600}$ mutations) signal as monomers, are Ras-independent, and are sensitive to current Raf monomer inhibitors such as vemurafenib or dabrafenib. Class 2 *BRAF* mutants signal as constitutive dimers, are Ras-independent, and are resistant to vemurafenib. Cells bearing these mutations may be sensitive to Raf dimer and/or MEK inhibitors. Class 3 mutants have low or absent protein kinase activity, are Ras-dependent, and are sensitive to ERK-dependent feedback of Ras. These mutations increase their binding to Ras and their activation requires coexistent mechanisms for Ras activation in the tumor cell in order to function. Class 3 mutants are not independent tumor drivers. Accordingly, they act as amplifiers of the Ras signal that are induced by *RAS* mutations, NF1 loss, or activation of receptors. Class 3 *BRAF* mutants coexist with mutations in *RAS* or *NF1* in melanomas; these tumors may be sensitive to MEK inhibitors. The majority of class 3 mutants in epithelial tumors (non-melanomas) are not associated with Ras/NF1 alterations and they may be effectively treated with targeted combinations that include inhibitors of the receptor protein-tyrosine kinases that are responsible for driving Ras activation. Selected Class1–3 mutations and their location within B-Raf are listed in Table 5.

The class 1 $BRAF^{V600E}$ mutation is the dominant mutation of this gene in human cancers [102]. This stimulatory mutation is located in the activation segment and its location suggests that it disrupts the structure of a dormant segment thereby converting it to an active conformation. The B-Raf^{V600E} mutant does not require Ras activity nor dimerization to assume an active state; the mutant monomer is functionally active. However, these mutants also have the potential to form homo- and heterodimers. Several class 2 mutations involve the proximal portion of the activation segment and are associated with high or intermediate activity. Although these mutants function as Ras-independent dimers, it is difficult to understand how mutations in the activation segment can promote side-to-side dimer formation owing to the distance of the mutant residues from the αC- and αE-helices and the β3-strand residues that make up the interface. It is possible that multiple distinct, but complementary, mechanisms are responsible for the activation of the class 2 mutants. Class 2 R462 and I463 mutations occur immediately before the G-rich loop, G464 is the first G-loop residue, and G469 occurs at the end of the loop. These have intermediate or high activity and function as dimers independent of Ras; because they possess significant catalytic activity, they have the potential to function as homodimers or as heterodimers with C-Raf. Class 3 G466 and S467 mutations occur near the end of the G-rich loop and have impaired activity; these mutants form Ras-dependent dimers. The G469 A/V/S mutant had high activity, but the G469E mutant has impaired activity. Mutations in the *BRAF* G-rich loop most likely function as an activator of C-Raf in a side-to-side heterodimerization manner thereby leading to increased MAP kinase pathway activity [83]. Additional biochemical and structural work will be required to define the precise mechanisms that these mutants use to promote MAP kinase pathway activation.

8. Epilogue

8.1. Amplification in the Ras-Raf-MEK-ERK signaling cascade

One theoretical consequence of a protein kinase signaling cascade is that of amplification. One protein kinase can conceivably catalyze the phosphorylation of thousands of protein substrate molecules. If the substrate is also a protein kinase, it can also catalyze the phosphorylation of thousands of substrate molecules, thereby leading to amplifications exceeding 1×10^6. Moreover, such regulatory amplifications can occur on a millisecond time scale [104]. The initial definition of a cascade is that of a series of waterfalls. The amount of water that goes over the last waterfall is the same as that going over the first waterfall and amplification does not occur. As noted next, however, amplification can occur in physiological signal-transduction cascades.

Fujioka et al. measured the content of Ras, Raf, MEK, and ERK in human HeLa cells. Note that the Raf content is much lower than that of the components of this signaling module and they found that the Ras content is 30-fold greater than that of Raf (Table 6) [105]. They also found that the MEK content is about 110 times that of Raf, but the ERK content is only 69% that of MEK. Thus, in the ERK signaling module, the potential of a 110-fold amplification from Raf to MEK is possible. In contrast, this degree of amplification from MEK to ERK is implausible. Fujioka et al. discovered that EGF stimulation of HeLa cells leads to the activation of 50% of Ras, 50% of Raf, 5% of MEK, and ≈ 60% of ERK. This finding demonstrates that EGF produced an approximate 10-fold amplification of MEK from Raf and an 8-fold amplification of MEK from ERK. These results show that a substantial 81-fold amplification from Raf to ERK occurred, but not a hypothetical increase of several orders of magnitude. For protein kinases in general, the concentration of the kinase and the kinase substrates are usually within one or two orders of magnitude of each other and overall pathway amplification is not as great as first imagined. These results emphasize the notion that protein kinases do not need high turnover numbers to function within the cell.

8.2. Resistance to the Raf and MEK1/2 inhibitors

As noted by Winer and colleagues “Biologically, the cancer cell is notoriously wily; each time we throw an obstacle in its path, it finds an alternate route that must then be blocked” [106]. Both vemurafenib and dabrafenib produce favorable responses in about 50% of melanoma patients with $BRAF^{V600E/K}$ mutations [42]. However, this indicates that 50% of such patients have primary resistance and the basis for this resistance is unknown. The ability of vemurafenib and dabrafenib to cause tumor regression in a large proportion of patients with BRAF-mutant advanced melanoma provides strong support for the notion that

Table 5
Classification of selected *BRAF* mutants[a].

Class	Mutation	Location of mutation	Kinase activity	Comments
1	V600E/K/D/R	Activation segment	High	Occurs most frequently in melanomas
2	R462I	G-rich loop	Intermediate	
2	I463S	G-rich loop	Intermediate	
2	G464E/V/R	G-rich loop	Intermediate	Breast cancer G464V
2	G469 A/V/S	G-rich loop	High/Intermediate	NSCLC G649 A; G649 V melanoma
2	E586K	β7–β8 loop	High	
2	F595L	DFG	Intermediate	
2	L597Q/R/S/V	Activation segment	High/ Intermediate	Melanoma L597R; NSCLC L597V
2	A598V	Activation segment	Active	
2	T599I	Activation segment	Intermediate	
2	K601E/N/T	Activation segment	High	Melanoma K601E
2	A727V	Distal to αI	Intermediate	
2	B-Raf fusions		High	
3	G466 A/E/V/R	G-rich loop	Impaired	Stomach cancer G466V
3	S467 A/E/L	G-rich loop	Impaired	
3	G469E	G-rich loop	Impaired	
3	K438M	Proximal to β1	Impaired	
3	D594 A/E/G/H/N/V	DFG	None	Melanoma D594N
3	G596 A/C/D/R	DFG	Impaired	Colorectal cancer G596R

[a] Data from Ref. [102].

Table 6
Concentration of Ras, Raf, MEK, and ERK in HeLa cells[a].

	Total (nM)	Activated (nM)[b]
Ras	400	200
Raf	13	6.5
MEK	1400	70
ERK	960	550

[a] Data from Ref. [105].
[b] Concentration of activated component following EGF stimulation.

the oncogenic B-RAF protein is a dominant driver of tumor growth and maintenance. However, the vast majority of benign cutaneous nevi harbor the same $BRAF^{V600E}$ mutation [107]. It appears that the *BRAF* mutation may be an initiating event in melanoma tumorigenesis. Our current understanding of melanocyte biology suggests that the nevi are benign because the *BRAF* mutation alone (without cooperating mutations) induces senescence [108]. That additional factors may be involved in the pathogenesis of melanomas may explain why only about one-half of all patients with advanced disease respond to these drugs.

In 132 patients with secondary, or acquired, resistance to vemurafenib (64% of patients) or dabrafenib (36%), resistance mechanisms were identified in 57% of these individuals [109]. The various secondary resistance mechanisms include *NRAS* or *KRAS* mutations (20%), *BRAF* splice variants (16%), $BRAF^{V600E/K}$ amplifications (13%), *MEK1/2* mutations (7%), and non-MAP kinase pathway alterations (11%). The non-MAP kinase pathway alterations include activation of the PI3 kinase/Akt pathway, amplification of the MITF transcription factor, and overexpression of PDGFR or the insulin-like growth factor receptor. It is likely that mechanisms for resistance to combined Raf and MEK inhibitors are similar to those described for Raf inhibitors [42]. In tumors other than melanomas possessing $BRAF^{V600E}$ mutations, such as in colorectal and thyroid cancers, the response rates to vemurafenib or dabrafenib inhibitors are low [58]. In comparison with melanoma, increased upstream receptor protein-tyrosine kinase expression and activity (mostly through EGFR in colorectal cancers and ErbB2/HER2–ErbB3/HER3 signaling in thyroid cancers) has been reported to account for the unexpected unresponsiveness. Following Raf inhibitor treatment, feedback reactivation of upstream receptors and Ras is more pronounced in these neoplasms thereby enhancing Raf dimerization and thus limiting the effect of αC_{out} inhibitors such as vemurafenib.

The MAP kinase pathway is evolutionarily conserved and the blockade of the pathway likely evokes many changes to restore pathway integrity. All cells including cancer cells typically express multiple receptor protein-tyrosine kinases that mediate signals that converge on essential downstream cell-survival effectors including the MAP kinase and PI3 kinase pathways. Accordingly, an increase in cytokines, growth factors, or hormones may confer drug resistance to inhibitors of oncogenic protein kinases that also activate the MAP kinase and PI3 kinase pathways. Wilson et al. studied a panel of ErbB2/HER amplified, EGFR mutated, MET amplified, PDGFR amplified, FGFR amplified, and *BRAF* mutated human cancer cell lines and discovered that most of them could be made resistant to previously inhibitory drugs by exposing them to one or more receptor ligands [110]. They examined the effects of six different receptor ligands that are widely expressed in various tumors including hepatocyte growth factor (HGF), EGFR, fibroblast growth factor, PDGF, neuregulin-1 (ligand for ErbB3/HER3 and ErbB4/HER4), and insulin-like growth factor. They found that HGF, fibroblast growth factor, and neuregulin-1 were the most broadly active ligands in promoting drug resistance followed by EGF. In contrast, insulin-like growth factor and PDGF had relatively little effect in these cell lines. These investigators discovered that HGF confers resistance to vemurafenib in *BRAF*-mutant melanoma cells.

In follow-up experiments, Caenepeel et al. examined three $BRAF^{V600E}$ melanoma cell lines to determine whether HGF would confer resistance to vemurafenib [111]. They discovered that vemurafenib blocked the proliferative capacity of all three cell lines and that HGF normalized cell proliferation in the presence of the B-Raf antagonist. They examined the effects of the receptor ligands listed in the previous paragraph on the ability to confer vemurafenib resistance and discovered that fibroblast growth factor conferred some resistance, but it was not as effective as HGF. These investigators also discovered that HGF also conferred drug resistance to dabrafenib and the combination of dabrafenib and trametinib in several patient-derived $BRAF^{V600E}$ cell lines. They also found that HGF conferred resistance against trametinib in four of six patient-derived *NRAS*-mutant cell lines. To confirm the role of MET signaling in mediating the HGF rescue, they discovered that a selective MET antagonist restored the vemurafenib antiproliferative effect. These workers discovered that vemurafenib treatment of mutant melanoma cells induced marked increases in MET and GAB1 transcript and protein levels. They found a significant increase in GAB1 (a MET adaptor protein) in response to a MEK inhibitor. Together, these results suggest that the increases in MET and GAB1 may ready *BRAF*-mutant cells for the HGF response. These studies suggest that the combination treatment with B-Raf, MEK, and MET inhibitors (such as crizotinib) might be efficacious in the treatment of *BRAF*-mutant melanomas.

Monitoring the levels of MET and tumor HGF may have clinical utility for identifying patients that are most likely to benefit from such combination therapy.

Because mutations, overexpression, and dysregulation of protein kinases play central roles in the pathogenesis of numerous human ailments including autoimmune, inflammatory, and nervous diseases as well as cancer, this enzyme family has become one of the most important drug targets during the past two dozen years [1,112]. Moreover, there are more than 175 different orally effective protein kinase inhibitors in clinical trials worldwide [113]; a complete listing can be found at www.icoa.fr/pkidb/. There are about three dozen FDA-approved medicines (www.brimr.org/PKI/PKIs.htm) that are directed against about 20 different protein kinases. Moreover, drugs targeting an additional 20 protein kinases are in clinical trials worldwide [30,113]. Owing to the hundreds of cancer amplicons and disease loci that have been mapped in the human genome [4], one can anticipate a substantial increase in the number of enzymes that will be targeted for the treatment of additional illnesses. Despite the success in the use of Raf and MEK targeted therapies in the treatment of melanoma as well as other targeted therapies in the treatment of other cancers, the almost universal development of drug resistance is a vexing problem that can only be solved with additional experimentation.

Conflict of interest

The author is unaware of any affiliations, memberships, or financial holdings that might be perceived as affecting the objectivity of this review.

Acknowledgments

The colored figures in this paper were evaluated to ensure that their perception was accurately conveyed to colorblind readers [114]. The author thanks Laura M. Roskoski for providing editorial and bibliographic assistance. We also thank Josie Rudnicki and Jasper Martinsek help in preparing the figures and Pasha Brezina and W.S. Sheppard for their help in structural analyses.

References

[1] R. Roskoski Jr., A historical overview of protein kinases and their targeted small molecule inhibitors, Pharmacol. Res. 100 (2015) 1–23.
[2] D. Fabbro, S.W. Cowan-Jacob, H. Moebitz, Ten things you should know about protein kinases: IUPHAR Review 14, Br. J. Pharmacol. 172 (2015) 2675–2700.
[3] A.J. Kooistra, A. Volkamer, Kinase-centric computational drug development, Ann. Rep. Med. Chem. 50 (2017) 197–236.
[4] G. Manning, D.B. Whyte, R. Martinez, T. Hunter, S. Sudarsanam, The protein kinase complement of the human genome, Science 298 (2002) 1912–1934.
[5] R. Roskoski Jr., RAF protein-serine/threonine kinases: structure and regulation, Biochem. Biophys. Res. Commun. 399 (2010) 313–317.
[6] R. Roskoski Jr., MEK1/2 dual-specificity protein kinases: structure and regulation, Biochem. Biophys. Res. Commun. 417 (2012) 5–10.
[7] M. Malumbres, M. Barbacid, RAS oncogenes: the first 30 years, Nat. Rev. Cancer 3 (2003) 459–465.
[8] A.G. Stephen, D. Esposito, R.K. Bagni, F. McCormick, Dragging Ras back in the ring, Cancer Cell 25 (2014) 272–281.
[9] D.K. Simanshu, D.V. Nissley, F. McCormick, RAS proteins and their regulators in human disease, Cell 170 (2017) 17–33.
[10] M. Holderfield, M.M. Deuker, F. McCormick, M. McMahon, Targeting RAF kinases for cancer therapy: BRAF-mutated melanoma and beyond, Nat. Rev. Cancer 14 (2014) 455–467.
[11] R. Roskoski Jr., ERK1/2 MAP kinases: structure, function, and regulation, Pharmacol. Res. 66 (2012) 105–143.
[12] D.A. Fruman, C. Rommel, PI3K and cancer: lessons, challenges and opportunities, Nat. Rev. Drug Discov. 13 (2014) 140–156.
[13] C.J. Caunt, M.J. Sale, P.D. Smith, S.J. Cook, MEK1 and MEK2 inhibitors and cancer therapy: the long and winding road, Nat. Rev. Cancer 15 (2015) 577–592.
[14] R. Roskoski Jr., Allosteric MEK1/2 inhibitors including cobimetanib and trametinib in the treatment of cutaneous melanomas, Pharmacol. Res. 117 (2017) 20–31.
[15] L.R. Gentry, T.D. Martin, D.J. Reiner, C.J. Der, Ral small GTPase signaling and oncogenesis: more than just 15minutes of fame, Biochim. Biophys. Acta 1843 (2014) 2976–2988.
[16] A.T. Baines, D. Xu, C.J. Der, Inhibition of Ras for cancer treatment: the search continues, Future Med. Chem. 3 (2011) 1787–1808.
[17] A.Q. Khan, S. Kuttikrishnan, K.S. Siveen, K.S. Prabhu, M. Shanmugakonar, H.A. Al-Naemi, et al., RAS-mediated oncogenic signaling pathways in human malignancies, Semin. Cancer Biol. (2018), https://doi.org/10.1016/j.semcancer.2018.03.001 pii: S1044-579X(18)30002-6 [Epub ahead of print].
[18] Y. Pylayeva-Gupta, E. Grabocka, D. Bar-Sagi, RAS oncogenes: weaving a tumorigenic web, Nat. Rev. Cancer 11 (2011) 761–774.
[19] A.A. Samatar, P.I. Poulikakos, Targeting RAS-ERK signalling in cancer: promises and challenges, Nat. Rev. Drug Discov. 13 (2014) 928–942.
[20] J.M. Ostrem, K.M. Shokat, Direct small-molecule inhibitors of KRAS: from structural insights to mechanism-based design, Nat. Rev. Drug Discov. 15 (2016) 771–785.
[21] A.V. Statsyuk, Let K-Ras activate its own inhibitor, Nat. Struct. Mol. Biol. (2018), https://doi.org/10.1038/s41594-018-0066-0 [Epub ahead of print].
[22] R. Hansen, U. Peters, A. Babbar, Y. Chen, J. Feng, M.R. Janes, et al., The reactivity-driven biochemical mechanism of covalent $KRAS^{G12C}$ inhibitors, Nat. Struct. Mol. Biol. (2018), https://doi.org/10.1038/s41594-018-0061-5.
[23] E. Hodis, I.R. Watson, G.V. Kryukov, S.T. Arold, M. Imielinski, J.P. Theurillat, et al., A landscape of driver mutations in melanoma, Cell 150 (2012) 251–263.
[24] Cancer Genome Atlas Network, Genomic classification of cutaneous melanoma, Cell 161 (2015) 1681–1696.
[25] H. Namba, M. Nakashima, T. Hayashi, N. Hayashida, S. Maeda, T.I. Rogounovitch, et al., Clinical implication of hot spot *BRAF* mutation, V599E, in papillary thyroid cancers, J. Clin. Endocrinol. Metab. 88 (2003) 4393–4397.
[26] J.C. Jones, L.A. Renfro, H.O. Al-Shamsi, A.B. Schrock, A. Rankin, B.Y. Zhang, et al., $^{Non-V600}$*BRAF* Mutations Define a Clinically Distinct Molecular Subtype of Metastatic Colorectal Cancer, J. Clin. Oncol. 35 (2017) 2624–2630.
[27] S. Cardarella, A. Ogino, M. Nishino, M. Butaney, J. Shen, C. Lydon, et al., Clinical, pathologic, and biologic features associated with *BRAF* mutations in non-small cell lung cancer, Clin. Cancer Res. 19 (2013) 4532–4540.
[28] P.K. Paik, M.E. Arcila, M. Fara, C.S. Sima, V.A. Miller, M.G. Kris, et al., Clinical characteristics of patients with lung adenocarcinomas harboring BRAF mutations, J. Clin. Oncol. 29 (2011) 2046–2051.
[29] H. Davies, G.R. Bignell, C. Cox, P. Stephens, S. Edkins, S. Clegg, et al., Mutations of the BRAF gene in human cancer, Nature 417 (2002) 949–954.
[30] P.M. Fischer, Approved and experimental small-molecule oncology kinase inhibitor drugs: a mid-2016 overview, Med. Res. Rev. 37 (2017) 314–367.
[31] T. Eisen, T. Ahmad, K.T. Flaherty, M. Gore, S. Kaye, R. Marais, et al., Sorafenib in advanced melanoma: a phase II randomised discontinuation trial analysis, Br. J. Cancer 95 (2006) 581–586.
[32] P.B. Chapman, A. Hauschild, C. Robert, J.B. Haanen, P. Ascierto, J. Larkin, et al., Improved survival with vemurafenib in melanoma with BRAF V600E mutation, N. Engl. J. Med. 364 (2011) 2507–2516.
[33] Y. Zhao, A.A. Adjei, The clinical development of MEK inhibitors, Nat. Rev. Clin. Oncol. 11 (2014) 385–400.
[34] A. Hauschild, J.J. Grob, L.V. Demidov, T. Jouary, R. Gutzmer, M. Millward, et al., Dabrafenib in *BRAF*-mutated metastatic melanoma: a multicentre, open-label, phase 3 randomised controlled trial, Lancet 380 (2012) 358–365.
[35] K.T. Flaherty, C. Robert, P. Hersey, P. Nathan, C. Garbe, M. Milhem, et al., Improved survival with MEK inhibition in BRAF-mutated melanoma, N. Engl. J. Med. 367 (2012) 107–114.
[36] K.B. Kim, R. Kefford, A.C. Pavlick, J.R. Infante, A. Ribas, J.A. Sosman, et al., Phase II study of the MEK1/MEK2 inhibitor trametinib in patients with metastatic *BRAF*-mutant cutaneous melanoma previously treated with or without a BRAF inhibitor, J. Clin. Oncol. 31 (2013) 482–489.
[37] K.T. Flaherty, J.R. Infante, A. Daud, R. Gonzalez, R.F. Kefford, J. Sosman, et al., Combined BRAF and MEK inhibition in melanoma with BRAF V600 mutations, N. Engl. J. Med. 367 (2012) 1694–1703.
[38] J. Larkin, P.A. Ascierto, B. Dréno, V. Atkinson, G. Liszkay, M. Maio, et al., Combined vemurafenib and cobimetinib in *BRAF*-mutated melanoma, N. Engl. J. Med. 371 (2014) 1867–1876.
[39] R. Dummer, P.A. Ascierto, H.J. Gogas, A. Arance, M. Mandala, G. Liszkay, et al., Encorafenib plus binimetinib versus vemurafenib or encorafenib in patients with *BRAF*-mutant melanoma (COLUMBUS): a multicentre, open-label, randomised phase 3 trial, Lancet Oncol. 19 (2018) 603–615.
[40] K.S. Smalley, Z. Eroglu, V.K. Sondak, Combination therapies for melanoma: a new standard of care? Am. J. Clin. Dermatol. 17 (2016) 99–105.
[41] P. Sharma, J.P. Allison, The future of immune checkpoint therapy, Science 348 (2015) 56–61.
[42] J.J. Luke, K.T. Flaherty, A. Ribas, G.V. Long, Targeted agents and immunotherapies: optimizing outcomes in melanoma, Nat. Rev. Clin. Oncol. 14 (2017) 463–482.
[43] H. Lavoie, M. Sahmi, P. Maisonneuve, S.A. Marullo, N. Thevakumaran, T. Jin, et al., MEK drives BRAF activation through allosteric control of KSR proteins, Nature 554 (2018) 549–553.
[44] D. Frodyma, B. Neilsen, D. Costanzo-Garvey, K. Fisher, R. Lewis, Coordinating ERK signaling via the molecular scaffold Kinase Suppressor of Ras, F1000Res 6 (2017) 1621, https://doi.org/10.12688/f1000research.11895.1 eCollection 2017.
[45] S.K. Hanks, T. Hunter, Protein kinases 6. The eukaryotic protein kinase superfamily: kinase (catalytic) domain structure and classification, FASEB J. 9 (1995) 576–596.
[46] D.R. Knighton, J.H. Zheng, L.F. Ten Eyck, V.A. Ashford, N.H. Xuong, S.S. Taylor, et al., Crystal structure of the catalytic subunit of cyclic adenosine monophosphate-dependent protein kinase, Science 253 (1991) 407–414.
[47] D.R. Knighton, J.H. Zheng, L.F. Ten Eyck, N.H. Xuong, S.S. Taylor, J.M. Sowadski,

Structure of a peptide inhibitor bound to the catalytic subunit of cyclic adenosine monophosphate-dependent protein kinase, Science 253 (1991) 414–420.
[48] R. Roskoski Jr., Src protein-tyrosine kinase structure, mechanism, and small molecule inhibitors, Pharmacol. Res. 94 (2015) 9–25.
[49] A.C. Bastidas, M.S. Deal, J.M. Steichen, Y. Guo, J. Wu, S.S. Taylor, Phosphoryl transfer by protein kinase A is captured in a crystal lattice, J. Am. Chem. Soc. 135 (2013) 4788–4798.
[50] M.J. Knape, F.W. Herberg, Metal coordination in kinases and pseudokinases, Biochem. Soc. Trans. 45 (2017) 653–663.
[51] R.S. Vijayan, P. He, V. Modi, K.C. Duong-Ly, H. Ma, J.R. Peterson, et al., Conformational analysis of the DFG-out kinase motif and biochemical profiling of structurally validated type II inhibitors, J. Med. Chem. 8 (58) (2015) 466–479.
[52] A. Haldane, W.F. Flynn, P. He, R.M. Levy, Coevolutionary landscape of kinase family proteins: sequence probabilities and functional motifs, Biophys. J. 114 (2018) 21–31.
[53] S.S. Taylor, M.M. Keshwani, J.M. Steichen, A.P. Kornev, Evolution of the eukaryotic protein kinases as dynamic molecular switches, Philos. Trans. R. Soc. Lond. B: Biol. Sci. 367 (2012) 2517–2528.
[54] B. Nolen, S. Taylor, G. Ghosh, Regulation of protein kinases; controlling activity through activation segment conformation, Mol. Cell 15 (2004) 661–675.
[55] D.J. Rawlings, A.M. Scharenberg, H. Park, M.I. Wahl, S. Lin, R.M. Kato, et al., Activation of BTK by a phosphorylation mechanism initiated by SRC family kinases, Science 271 (1996) 822–825.
[56] B.H. Zhang, K.L. Guan, Activation of B-Raf kinase requires phosphorylation of the conserved residues Thr598 and Ser601, EMBO J. 19 (2000) 5429–5439.
[57] J. Zhou, J.A. Adams, Participation of ADP dissociation in the rate-determining step in cAMP-dependent protein kinase, Biochemistry 36 (1997) 15733–15738.
[58] Z. Karoulia, E. Gavathiotis, P.I. Poulikakos, New perspectives for targeting RAF kinase in human cancer, Nat. Rev. Cancer 17 (676) (2017).
[59] D.F. Brennan, A.C. Dar, N.T. Hertz, W.C. Chao, A.L. Burlingame, K.M. Shokat, et al., A Raf-induced allosteric transition of KSR stimulates phosphorylation of MEK, Nature 472 (2011) 366–369.
[60] A.P. Kornev, N.M. Haste, S.S. Taylor, L.F. Ten Eyck, Surface comparison of active and inactive protein kinases identifies a conserved activation mechanism, Proc. Natl. Acad. Sci. U. S. A. 103 (2006) 17783–17788.
[61] A.P. Kornev, S.S. Taylor, L.F. Ten Eyck, A helix scaffold for the assembly of active protein kinases, Proc. Natl. Acad. Sci. U. S. A. 105 (2008) 14377–14382.
[62] R. Roskoski Jr., Anaplastic lymphoma kinase (ALK): structure, oncogenic activation, and pharmacological inhibition, Pharmacol. Res. 68 (2013) 68–94.
[63] R. Roskoski Jr., Anaplastic lymphoma kinase (ALK) inhibitors in the treatment of ALK-driven lung cancers, Pharmacol. Res. 117 (2017) 343–356.
[64] R. Roskoski Jr., Cyclin-dependent protein kinase inhibitors including palbociclib as anticancer drugs, Pharmacol. Res. 111 (2016) 784–803.
[65] R. Roskoski Jr., ErbB/HER protein-tyrosine kinases: structures and small molecule inhibitors, Pharmacol. Res. 79 (2014) 34–74.
[66] R. Roskoski Jr., Janus kinase (JAK) inhibitors in the treatment of inflammatory and neoplastic diseases, Pharmacol. Res. 111 (2016) 784–803.
[67] R. Roskoski Jr., The role of small molecule Kit protein-tyrosine kinase inhibitors in the treatment of neoplastic disorders, Pharmacol. Res. 133 (2018) 35–52.
[68] R. Roskoski Jr., The role of small molecule platelet-derived growth factor receptor (PDGFR) inhibitors in the treatment of neoplastic disorders, Pharmacol. Res. 129 (2018) 65–83.
[69] R. Roskoski Jr., A. Sadeghi-Nejad, Role of RET protein-tyrosine kinase inhibitors in the treatment RET-driven thyroid and lung cancers, Pharmacol. Res. 128 (2018) 1–17.
[70] R. Roskoski Jr., ROS1 protein-tyrosine kinase inhibitors in the treatment of ROS1 fusion protein-driven non-small cell lung cancers, Pharmacol. Res. 121 (2017) 202–212.
[71] M.C. Frame, R. Roskoski Jr., Src family tyrosine kinases, Reference Module in Life Sciences, Elsevier, Amsterdam, 2017, pp. 1–11, https://doi.org/10.1016/B978-0-12-809633-8.07199-5.
[72] R. Roskoski Jr., Vascular endothelial growth factor (VEGF) and VEGF receptor inhibitors in the treatment of renal cell carcinomas, Pharmacol. Res. 120 (2017) 116–132.
[73] H.S. Meharena, P. Chang, M.M. Keshwani, K. Oruganty, A.K. Nene, N. Kannan, et al., Deciphering the structural basis of eukaryotic protein kinase regulation, PLoS Biol. 11 (2013) e1001690.
[74] P.M. Ung, R. Rahman, A. Schlessinger, Redefining the protein kinase conformational space with machine learning, Cell Chem. Biol. 25 (2018) 916-924.e2.
[75] K. Shah, Y. Liu, C. Deirmengian, K.M. Shokat, Engineering unnatural nucleotide specificity for Rous sarcoma virus tyrosine kinase to uniquely label its direct substrates, Proc. Natl. Acad. Sci. U. S. A. 94 (1997) 3565–3570.
[76] Y. Liu, K. Shah, F. Yang, L. Witucki, K.M. Shokat, A molecular gate which controls unnatural ATP analogue recognition by the tyrosine kinase v-Src, Bioorg. Med. Chem. Lett. 6 (1998) 1219–1226.
[77] J.J. Liao, Molecular recognition of protein kinase binding pockets for design of potent and selective kinase inhibitors, J. Med. Chem. 50 (2007) 409–424.
[78] R. Roskoski Jr., Classification of small molecule protein kinase inhibitors based upon the structures of their drug-enzyme complexes, Pharmacol. Res. 103 (2016) 26–48.
[79] J. Hu, H. Yu, A.P. Kornev, J. Zhao, E.L. Filbert, S.S. Taylor, A.S. Shaw, Mutation that blocks ATP binding creates a pseudokinase stabilizing the scaffolding function of kinase suppressor of Ras, CRAF and BRAF, Proc. Natl. Acad. Sci. U. S. A. 108 (2011) 6067–6072.
[80] P.T. Wan, M.J. Garnett, S.M. Roe, S. Lee, D. Niculescu-Duvaz, V.M. Good, et al., Mechanism of activation of the RAF-ERK signaling pathway by oncogenic mutations of B-RAF, Cell 116 (2004) 855–867.
[81] M.M. McKay, D.A. Ritt, D.K. Morrison, Signaling dynamics of the KSR1 scaffold complex, Proc. Natl. Acad. Sci. U. S. A. 106 (2009) 11022–11027.
[82] T. Rajakulendran, M. Sahmi, M. Lefrançois, F. Sicheri, M. Therrien, A dimerization-dependent mechanism drives RAF catalytic activation, Nature 461 (2009) 542–545.
[83] J.R. Haling, J. Sudhamsu, I. Yen, S. Sideris, W. Sandoval, W. Phung, et al., Structure of the BRAF-MEK complex reveals a kinase activity independent role for BRAF in MAPK signaling, Cancer Cell 26 (2014) 402–413.
[84] A.C. Dar, K.M. Shokat, The evolution of protein kinase inhibitors from antagonists to agonists of cellular signaling, Annu. Rev. Biochem. 80 (2011) 769–795.
[85] J. Monod, J.P. Changeux, F. Jacob, Allosteric proteins and cellular control systems, J. Mol. Biol. 6 (1963) 306–329.
[86] F. Zuccotto, E. Ardini, E. Casale, M. Angiolini, Through the "gatekeeper door": exploiting the active kinase conformation, J. Med. Chem. 53 (2010) 2691–2694.
[87] L.K. Gavrin, E. Saiah, Approaches to discover non-ATP site inhibitors, Med. Chem. Res. 4 (2013) 41.
[88] V. Lamba, I. Ghosh, New directions in targeting protein kinases: focusing upon true allosteric and bivalent inhibitors, Curr. Pharm. Des. 18 (2012) 2936–2945.
[89] F.E. Kwarcinski, K.R. Brandvold, S. Phadke, O.M. Beleh, T.K. Johnson, J.L. Meagher, et al., Conformation-selective analogues of dasatinib reveal insight into kinase inhibitor binding and selectivity, ACS Chem. Biol. 11 (2016) 1296–1304.
[90] Z. Zhao, H. Wu, L. Wang, Y. Liu, S. Knapp, Q. Liu, N.S. Gray, Exploration of type II binding mode: a privileged approach for kinase inhibitor focused drug discovery? ACS Chem. Biol. 9 (2014) 1230–1241.
[91] D. Bajusz, G.G. Ferenczy, G.M. Keserá, Structure-based virtual screening approaches in kinase-directed drug discovery, Curr. Top. Med. Chem. 17 (2017) 2235–2259.
[92] O.P. van Linden, A.J. Kooistra, R. Leurs, I.J. de Esch, C. de Graaf, KLIFS: a knowledge-based structural database to navigate kinase-ligand interaction space, J. Med. Chem. 57 (2014) 249–277.
[93] G. Bollag, J. Tsai, J. Zhang, C. Zhang, P. Ibrahim, K. Nolop, et al., Vemurafenib: the first drug approved for *BRAF*-mutant cancer, Nat. Rev. Drug Discov. 11 (2012) 873–886.
[94] T.R. Rheault, J.C. Stellwagen, G.M. Adjabeng, K.R. Hornberger, K.G. Petrov, A.G. Waterson, et al., Discovery of dabrafenib: a selective inhibitor of Raf kinases with antitumor activity against B-Raf-driven tumors, ACS Med. Chem. Lett. 4 (2013) 358–362.
[95] S.M. Wilhelm, C. Carter, L. Tang, D. Wilkie, A. McNabola, H. Rong, et al., BAY 43-9006 exhibits broad spectrum oral antitumor activity and targets the RAF/MEK/ERK pathway and receptor tyrosine kinases involved in tumor progression and angiogenesis, Cancer Res. 64 (2004) 7099–7109.
[96] S. Wilhelm, C. Carter, M. Lynch, T. Lowinger, J. Dumas, R.A. Smith, et al., Discovery and development of sorafenib: a multikinase inhibitor for treating cancer, Nat. Rev. Drug Discov. 5 (2006) 835–844 Erratum in: Nat Rev Drug Discov 2007;6:126.
[97] J.R. Henry, M.D. Kaufman, S.B. Peng, Y.M. Ahn, T.M. Caldwell, L. Vogeti, et al., Discovery of 1-(3,3-dimethylbutyl)-3-(2-fluoro-4-methyl-5-(7-methyl-2-(methylamino)pyrido[2,3-d]pyrimidin-6-yl)phenyl)urea (LY3009120) as a pan-RAF inhibitor with minimal paradoxical activation and activity against BRAF or RAS mutant tumor cells, J. Med. Chem. 58 (2015) 4165–4179.
[98] S.B. Peng, J.R. Henry, M.D. Kaufman, W.P. Lu, B.D. Smith, S. Vogeti, et al., Inhibition of RAF isoforms and active dimers by LY3009120 leads to anti-tumor activities in *RAS* or *BRAF* mutant cancers, Cancer Cell 28 (2015) 384–398.
[99] S.H. Chen, Y. Zhang, R.D. Van Horn, T. Yin, S. Buchanan, V. Yadav, et al., Oncogenic *BRAF* deletions that function as homodimers and are sensitive to inhibition by RAF dimer inhibitor LY3009120, Cancer Discov. 6 (2016) 300–315.
[100] C. Zhang, W. Spevak, Y. Zhang, E.A. Burton, Y. Ma, G. Habets, et al., RAF inhibitors that evade paradoxical MAPK pathway activation, Nature 526 (2015) 583–586.
[101] Z. Tang, X. Yuan, R. Du, S.H. Cheung, G. Zhang, J. Wei, et al., BGB-283, a novel RAF kinase and EGFR inhibitor, displays potent antitumor activity in *BRAF*-mutated colorectal cancers, Mol. Cancer Ther. 14 (2015) 2187–2197.
[102] M. Dankner, A.A.N. Rose, S. Rajkumar, P.M. Siegel, I.R. Watson, Classifying BRAF alterations in cancer: new rational therapeutic strategies for actionable mutations, Oncogene 37 (2018) 3183–3199.
[103] Z. Yao, R. Yaeger, V.S. Rodrik-Outmezguine, A. Tao, N.M. Torres, M.T. Chang, et al., Tumours with class 3 BRAF mutants are sensitive to the inhibition of activated RAS, Nature 548 (2017) 234–238.
[104] E.R. Stadtman, P.B. Chock, Interconvertible enzyme cascades in metabolic regulation, Curr. Top. Cell. Regul. 13 (1978) 53–95.
[105] A. Fujioka, K. Terai, R.E. Itoh, K. Aoki, T. Nakamura, S. Kuroda, et al., Dynamics of the Ras/ERK MAPK cascade as monitored by fluorescent probes, J. Biol. Chem. 281 (2006) 8917–8926.
[106] E. Winer, J. Gralow, L. Diller, B. Karlan, P. Loehrer, L. Pierce, et al., Clinical cancer advances 2008: major research advances in cancer treatment, prevention, and screening–a report from the American Society of Clinical Oncology, J. Clin. Oncol. 27 (2009) 812–826 Erratum in: J Clin Oncol 2009;27:3070–1.
[107] P.M. Pollock, U.L. Harper, K.S. Hansen, L.M. Yudt, M. Stark, C.M. Robbins, et al., High frequency of *BRAF* mutations in nevi, Nat. Genet. 33 (2003) 19–20.
[108] C. Michaloglou, L.C. Vredeveld, M.S. Soengas, C. Denoyelle, T. Kuilman, C.M. van der Horst, et al., $BRAF^{E600}$-associated senescence-like cell cycle arrest of human naevi, Nature 436 (2005) 720–724.
[109] D.B. Johnson, A.M. Menzies, L. Zimmer, Z. Eroglu, F. Ye, S. Zhao, et al., Acquired BRAF inhibitor resistance: a multicenter meta-analysis of the spectrum and

frequencies, clinical behaviour, and phenotypic associations of resistance mechanisms, Eur. J. Cancer 51 (2015) 2792–2799.
[110] T.R. Wilson, J. Fridlyand, Y. Yan, E. Penuel, L. Burton, E. Chan, et al., Widespread potential for growth-factor-driven resistance to anticancer kinase inhibitors, Nature 487 (2012) 505–509.
[111] S. Caenepeel, K. Cooke, S. Wadsworth, G. Huang, L. Robert, B.H. Moreno, et al., MAPK pathway inhibition induces MET and GAB1 levels, priming BRAF mutant melanoma for rescue by hepatocyte growth factor, Oncotarget 8 (2017) 17795–17809.
[112] P. Cohen, Protein kinases – the major drug targets of the twenty-first century? Nat. Rev. Drug Discov. 1 (2002) 309–315.
[113] F. Carles, S. Bourg, C. Meyer, P. Bonnet, PKIDB: a curated, annotated and updated database of protein kinase inhibitors in clinical trials, Molecules 23 (4) (2018), https://doi.org/10.3390/molecules23040908 pii: E908.
[114] R. Roskoski Jr., Guidelines for preparing color figures for everyone including the colorblind, Pharmacol. Res. 119 (2017) 240–241.